MASTERS DISSERTATION

GAS ENGINE OXYFUEL COMBUSTION FOR COMBINED HEAT AND POWER APPLICATIONS

BY

ANDREW CANTANHEDE CARDOSO

UNIVERSITY OF BRASÍLIA

FACULTY OF TECHNOLOGY

DEPARTMENT OF MECHANICAL ENGINEERING

UNIVERSITY OF BRASÍLIA
FACULTY OF TECHNOLOGY
DEPARTMENT OF MECHANICAL ENGINEERING

MASTERS DISSERTATION

GAS ENGINE OXYFUEL COMBUSTION FOR COMBINED HEAT AND POWER APPLICATIONS

A Dissertation Presented to the
Department of Mechanical Engineering

by

Andrew Cantanhede Cardoso

In Partial Fulfillment
of the Requirements for the Degree of
Master in Mechanical Science

Supervisor: Prof. Carlos Alberto Gurgel Veras, Ph.D.

PUBLICAÇÃO ENM.DM - XXX/AAAA
BRASÍLIA-DF, OCTOBER 31st 2022.

UNIVERSITY OF BRASÍLIA
FACULTY OF TECHNOLOGY
DEPARTMENT OF MECHANICAL ENGINEERING

MASTERS DISSERTATION

GAS ENGINE OXYFUEL COMBUSTION FOR COMBINED HEAT AND POWER APPLICATIONS

Approved by:

Prof. Carlos Alberto Gurgel Veras, Ph.D. - Advisor
ENM-UnB

Prof. Mario Baptista Benjamin Siqueira, Ph.D. - Internal Examiner
ENM-UnB

Prof. Fabio Cordeiro de Lisboa. - External Examiner
FGA-UnB

Prof. Guenther Carlos Krieger Filho, Ph.D. - External Examiner
Escola Politécnica - USP

BRASÍLIA-DF, 31 DE OUTUBRO DE 2022.

FICHA CATALOGRÁFICA
ANDREW CANTANHEDE CARDOSO
GAS ENGINE OXY FUEL COMBUSTION FOR COMBINED HEAT AND POWER APPLICATIONS
2022xv, 75p., 201x297 mm
(ENM/FT/UnB, Mestre, Engenharia Mecânica, 2022)
Dissertação de Mestrado - Universidade de Brasília - Faculdade de Tecnologia
Departamento de Engenharia Mecânica

REFERÊNCIA BIBLIOGRÁFICA

ANDREW CANTANHEDE CARDOSO (2022) Gas Engine OxyFuel Combustion for Combined Heat and Power Applications. Dissertação de Mestrado em Engenharia Mecânica, Publicação xxx/AAAA, Departamento de Engenharia Mecânica, Universidade de Brasília, Brasília, DF, 75p.

CESSÃO DE DIREITOS

AUTOR: Andrew Cantanhede Cardoso
TÍTULO: Gas Engine OxyFuel Combustion for Combined Heat and Power Applications
GRAU: Mestre
ANO: 2022

Andrew Cantanhede Cardoso
andrewccardoso@gmail.com

Acknowledgment

This acknowledgment chapter is written in Portuguese to properly pay tribute to those who captured the essence of partnership, loyalty, and friendship. My kindest regards!

Antes de tudo, agradeço ao Criador por ter proporcionado saúde durante o cumprimento de mais esta jornada. Conseguir ter meus pais ao meu lado mesmo diante dos graves problemas de ordem pessoal logo após a minha graduação, e, posteriormente, termos atravessado a maior crise sanitária dos últimos tempos com vida é algo confortante e recompensador. Obrigado Senhor!

Obrigado também aos amigos profissionais de Saúde, em especial Dr. Felipe, Dr. Marcos, Dr. Sérgio, Dr. Vinnicius, Dr. Wady e Dr. Rogério. Guardo-lhes no coração por tudo que vocês e suas equipes fizeram!

Agradeço aos meus pais Reynaldo e Mira, por serem um porto-seguro nos momentos difíceis; pela capacidade de tolerarem – na vida e em minhas obras com quatro rodas – as chatices de um engenheiro perfeccionista (ou melhor, de um Engenheiro Mecânico com alma de artista); pela troca de experiências de vida que sempre me permitem enxergar além e por tornarem-me uma pessoa melhor consigo e com o próximo. Sou grato a Deus pelo tesouro que vocês representam em minha vida!

A minha amada avó Lia (*in memoriam*, quanta saudade), à minha prima Dayse e ao meu querido tio Kid, que me motivaram a entregar sempre meu melhor em diversas circunstâncias da vida. *No pain, no gain*. Tio Kid, obrigado também por ajudar-me naquela época dolorida.

Àqueles com os quais tive o prazer da companhia e que não estão mais em nosso plano, em especial ao também Engenheiro Mecânico, grande mentor e caro professor de física nos meus tempos de Galois, Wagih Rassi Junior (*in memoriam*), e ao amigo de graduação em Engenharia Mecânica, Luís Felipe Veloso Carvalho da Silva (*in memoriam*). Aos familiares, sintam-se abraçados e confortados.

Aos amigos de ontem e de hoje: obrigado por compartilharmos os momentos alegres, por participarmos e vencermos várias das batalhas juntos – e perdermos algumas outras, faz parte, rs. – e pelas confidências, principalmente na época do erudito Galois. Bons tempos aqueles, hoje maturados em barris de carvalho!! Menciono aqui apenas alguns: o *alter ego* desde os três de idade – o sumido Guilherme – Felipe, Gabriel e Victor. Faço votos que nossas amizades perdurem por vindouros anos.

À Universidade de Brasília – UnB, em especial ao Departamento de Engenharia

Mecânica, tendo me acolhido em duas oportunidades: a primeira, num agora longínquo ano de 2010 como estudante de graduação, ocasião à qual tive ainda mais moldada minha personalidade e quando fiz ótimos colegas de profissão, inumeráveis nesta singela homenagem; e a segunda neste mestrado, sinal de que o bom filho a casa torna, provando mais uma vez àqueles de fora que, a despeito de tudo de pernicioso e preconceituoso possam imaginar, também fazemos Engenharia e Ciência em Brasília – Distrito Federal. "♪ *Neste país lugar melhor não há* ♫".

Ao Darío Gerardo Fantini pela sua formidável ajuda na disciplina de métodos numéricos. ¡*Muchas gracias, hermano*!

Aos amigos os quais sou grato por compartilharem o insaciável entusiasmo nato desta Capital pelo automóvel e automobilismo, dentre eles Fernando, Gilman, Zé Augusto, João, Dudu, Mazinho, Rosito, Renato e Wagnei. Quem sabe ano que vem estaremos de volta com o V8 no Autódromo de Brasília...Sonhemos, oremos e aguardemos.

Aos nobilíssimos Magistrados do Tribunal de Justiça do Distrito Federal e dos Territórios (TJDFT) por depositarem a mais alta confiança em mim nas mais de cinquenta nomeações e nas diversas avaliações periciais executadas no campo de Engenharia Mecânica, sobretudo aquelas no segmento automotivo, área que muito me apraz. Nesse contexto, faço uma menção especial aos Doutos(as) Juízes(as) da 22ª Vara Cível de Brasília, da 6ª Vara Cível de Brasília, da 2ª Vara Cível de Taguatinga, da Vara Cível do Guará, da 16ª Vara Cível de Brasília e da 23ª Vara Cível de Brasília. Tem sido uma enorme honra poder colaborar com a Justiça, e fico à disposição sempre que necessário for. Meu muitíssimo obrigado!

Ao estimado Professor Doutor Carlos Alberto Gurgel Veras: mais do que orientador deste trabalho, o senhor demonstrou um altruísmo ímpar ao abraçar-me no retorno à UnB, após eu expor qual era minha situação naquele momento e de minhas razões de não ter seguido no mestrado imediatamente após minha graduação. Agradeço ao senhor pelos esforços empenhados na condução da pesquisa e por seu alto espírito de profissionalismo, sendo um exemplo para o Departamento de Engenharia Mecânica (ENM-UnB), para a Universidade de Brasília como um todo e para este País. A cena acadêmica é grata por tê-lo na ativa e sou agradecido por sua compreensão, paciência e amizade. Fique certo que seu modelo reverberará sempre em minha vida, e serei feliz se algum dia puder seguir seus passos e tornar-me um mestre querido e respeitado tanto por meus pares, quanto pelos discentes. Parabéns por abraçar com tanto ímpeto esta nobre missão!

TABLE OF CONTENTS

LIST OF FIGURES

LIST OF TABLES

LIST OF SYMBOLS

Lowercase Latin letters

$c_P\|_0^t$	*mean mass specific heat at constant pressure*
$c_v\|_0^t$	*mean mass specific heat at constant volume*
c_P	*specific heat at constant pressure*
c_v	*specific heat at constant pressure*
h	*enthalpy*
h_{inAir}	*enthalpy intake fresh air*
h_{inT}	*enthalpy of exhaust gases in turbine*
k_c	*convenience coefficient*
k_s	*convenience coefficient "dry dissipation"*
k_w	*convenience coefficient "viscous dissipation"*
m	*in cylinder fluid mass*
m_{oxi}	*in cylinder oxidizer mass*
m_{fuel}	*in cylinder fuel mass*
m_a	*products mass*
$m_{O_2}^a$	*oxygen mass in products*
$\dot{m}_a$	*intake mass flow*
$\dot{m}_{eg}$	*exhaust mass flow*
m_{a1}	*air/fuel stoichiometric ratio*
n_1	*number of moles*
n_{cyl}	*number of cylinders*
p_e	*exhaust pressure*
$\bar{p}_c$	*mean compression pressure*
$\bar{p}_e$	*mean effective pressure*
$\bar{p}_{f,0}$	*constant mean pressure due to "dry" friction*
pmf_0	*constant mean pressure due to "dry" friction*
$\bar{p}_i$	*indicated mean pressure*

r	*charging coefficient*
rpm	*engine speed rotations per minute*
v	*specific volume*
w	*mean piston speed*

Uppercase Latin letters

AF_{act}	*Actual Air/Fuel ratio*
AF_{stoic}	*Stoichiometric Air/Fuel ratio*
AFR_{mb}	*Air/Fuel ratio mass based*
AFR_{vb}	*Air/Fuel ratio volumetric based*
$C_P\|_0^t$	*mean specific molar heat at constant pressure*
C_P	*specific molar heat at constant pressure*
D	*piston bore*
LHV	*lower heating value*
N	*Number of engine strokes*
P	*Atmospheric pressure*
P_{fuel}	*Fuel pressure*
P_e	*effective power*
PMI	*Bottom dead center*
PMS	*Top dead center*
Q	*Heat*
Q_E	*Heat at the exhaust*
R	*ideal gas law constant (mass)*
SFC	*Brake specific fuel consumption*
T	*Absolute temperature*
T_{inAir}	*Absolute temperature of air during intake*
T_{outAir}	*Absolute temperature of air exiting turbocharger*
T_{fuel}	*Absolute temperature of fuel*
T_{ref}	*Reference temperature*
U	*Internal energy*
V	*Volume*
V_1	*Volume at state 1 (beginning of compression)*
V_2	*Volume at state 2 (end of compression)*

V_{a1}	*Volume based air/fuel stoichiometric ratio*
V_{eng}	*Engine displacement*
V_{cyl}	*Cylinder displacement*
W_e	*Effective work*
W_R	*Breathing work*
W_{th}	*Theoretical work per cycle*
$Y_{O_2}^a$	*fraction of combustion products*

Lowercase Greek letters

α	*Nitrogen mole fraction*
β	*Carbon dioxide mole fraction*
γ	*Poisson coefficient in an ideal gas*
ε_{exh}	*Exhaust gases energy*
ε_{inw}	*Loss coefficient from intake work*
ε_P	*Cylinder walls heat transfer loss coefficient*
ε_R	*Breathing work loss coefficient*
ε_{wht}	*Loss coefficient from heat transfer to the walls*
ζ	*Convenience variable*
η_e	*Engine's effective efficiency*
η_i	*Cycle's internal efficiency*
η_{ind}	*Engine's indicated efficiency*
η_{mec}	*Engine's mechanical efficiency*
η_{isC}	*Isentropic compression efficiency (compressor wheel)*
η_{isT}	*Isentropic expansion efficiency (turbine wheel)*
η_{th}	*Theoretical cycle efficiency*
λ	*lambda air/fuel ratio*
ξ	*Convenience index (cycle integration of* $\overline{\gamma - 1}$
ρ	*Density*
ρ_0	*Density of the mix*
ρ_c	*Fuel density*
φ	*Volumetric heat flow*
χ	*Static compression ratio*
ψ	*Convenience variable*
ω	*Angular velocity*

Uppercase Greek letters

ΔP_{inw}	*Pressure variation during intake work*
Γ	*Oxygen molar fraction*
Φ	*Equivalence ratio*

RESUMO

A queima de hidrocarbonetos com oxigênio puro (*oxyfuel combustion*) remete ao processo de combustão no qual o comburente é, via de regra, uma mistura de oxigênio e CO_2. A técnica permite implementar processos de captura e armazenagem de carbono. Assim, objetivos principais deste estudo foram avaliar a oxi-combustão aplicada em plantas de cogeração baseadas em motores a gás. Os motores empregam gás de pirólise de resíduos sólidos urbanos como combustível. O calor rejeitado pela planta de potência sustenta as reações de pirólise do substrato sólido. Para tal, foi desenvolvido um modelo matemático e numérico para analisar o desempenho termoeconômico da planta de cogeração. A presença de dióxido de carbono nos reagentes reduz a temperatura da mistura após a compressão em aproximadamente 200 K comparado à combustão convencional, permitindo o motor operar com elevadas taxas compressão, ampliando os limites da detonação. As predições numéricas indicaram eficiência térmica do motor, operando no modo *oxyfuel*, sempre superior a 42%, similar a queima do gás de pirólise com ar atmosférico. A temperatura de descarga do motor predita pelo modelo varia de 512 a 799 °C na oxicombustão comparada a 962 °C da queima com ar atmosférico, sendo adequada para sustentar as reações de degradação térmica do combustível derivado de resíduos, viabilizando a planta de cogeração. Uma planta CHP-CCS produzindo 200 MW de potência elétrica, a um custo aproximado de 510 milhões de dólares, possui tempo de período de retorno de investimento em menos de 5 anos, capturando cerca de 1.1 milhões de toneladas de CO_2 por ano.

Palavras-chave: oxi-combustão, *oxyfuel*, motores de combustão interna, ciclo Otto, motor a gás, CHP, análise de viabilidade., gás de pirólise de lixo, RDF.

ABSTRACT

The burning of hydrocarbons with pure oxygen – called oxyfuel combustion – refers to the process of combustion in which the oxidizer is, as a rule, a mixture of oxygen and CO_2. This technique allows the implementation of carbon capture and storage processes. Thus, the main objectives of this study were to evaluate oxyfuel in cogeneration plants applied to gas engines. The engines use pyrolysis gases from municipal solid waste as fuel. Heat rejected by the power plant sustains the pyrolysis reactions of the solid substrate. To this end, a mathematical and numerical model were developed to analyze the thermoeconomic performance of the cogeneration plant. It was analyzed the influence of CO_2 concentration in oxidizer on engine exhaust temperature. The presence of carbon dioxide in reactants lowers in-chamber temperature during compression and power strokes at around 200 K when compared to conventional air combustion, minimizing knock tendency and allowing engine operation at higher compression ratios. Numerical predictions pointed a consistent 42% engine's thermal efficiency operating on oxyfuel mode, similar to RDF conventional air combustion. Engine's exhaust temperature obtained from the model varies from 512 to 799 °C on oxyfuel modes compared to 962 °C when in Conventional Air Combustion. This temperature level is appropriate to sustain refuse-derived fuel thermal decay reactions, thus enabling the cogeneration plant. A simulated CHP-CCS powerplant producing 200 MW electric power output at an approximate cost of US$ 510 million has a payback period of less than 5 years, capturing about 1.1 million tons of CO_2 per year.

Keywords: oxyfuel, internal combustion engine generator, Otto cycle, gas engine, CHP, feasibility analysis, Refuse-derived fuel., RDF.

Chapter 1

1 INTRODUCTION

This chapter is structured in four sections which present, respectively, a brief contextualization of the background and motivation related to this study, the research objectives, and a preview of the following chapters.

1.1 BACKGROUND AND MOTIVATION

As recent environmental concerns due to climate changes become even more relevant, other important correlated issues also need attention. On economic scale, the devastating COVID-19 pandemic and war on Ukraine accentuated fuel prices and energy generation costs, challenges consistently linked to geopolitical factors.

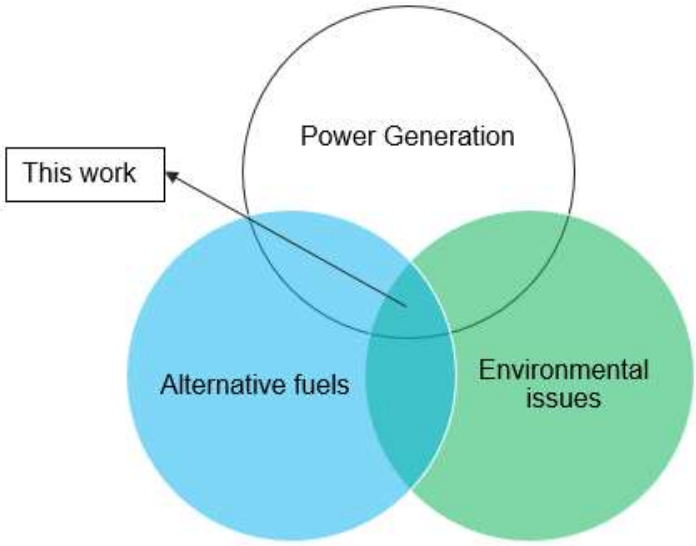

Figure 1 – Venn diagram of the ongoing global energy and environmental concerns. This work evaluates a solution addressed to the intersection area.

At every energy calamity following 70's oil crisis, new research on alternative fuel studies emerge aiming to find renewable sources [1]. Nowadays, there is a pressing need for reduction in greenhouse gas emissions and advanced burning technologies to reduce NO_x, carbon monoxide (CO), and hydrocarbons (HC) concentration in the flue gas. The European

Union, for instance, has defined ambitious targets for 2030, cutting no less than 40% in greenhouse gas emissions (CO_2, CH_4, N_2O, etc.) from 1990 levels, and improving around 32% overall energy transformation efficiency [2]. A major issue also linked to pollution is the relation with diseases and mutations that could eventually lead to birth defects, respiratory and circulatory disorders, and even cancer. [3]

Another relevant concern for the 21st century is the necessity to improve solid waste management and the possibility to transform waste into useful fuel for power generation without penalizing long-term environmental perspectives. There is a need, however, to mature a set of technologies that could exploit this huge energy source as depicted in Fig. 2. Advanced technologies for waste to energy conversion power plants are pyrolysis and plasma gasification.

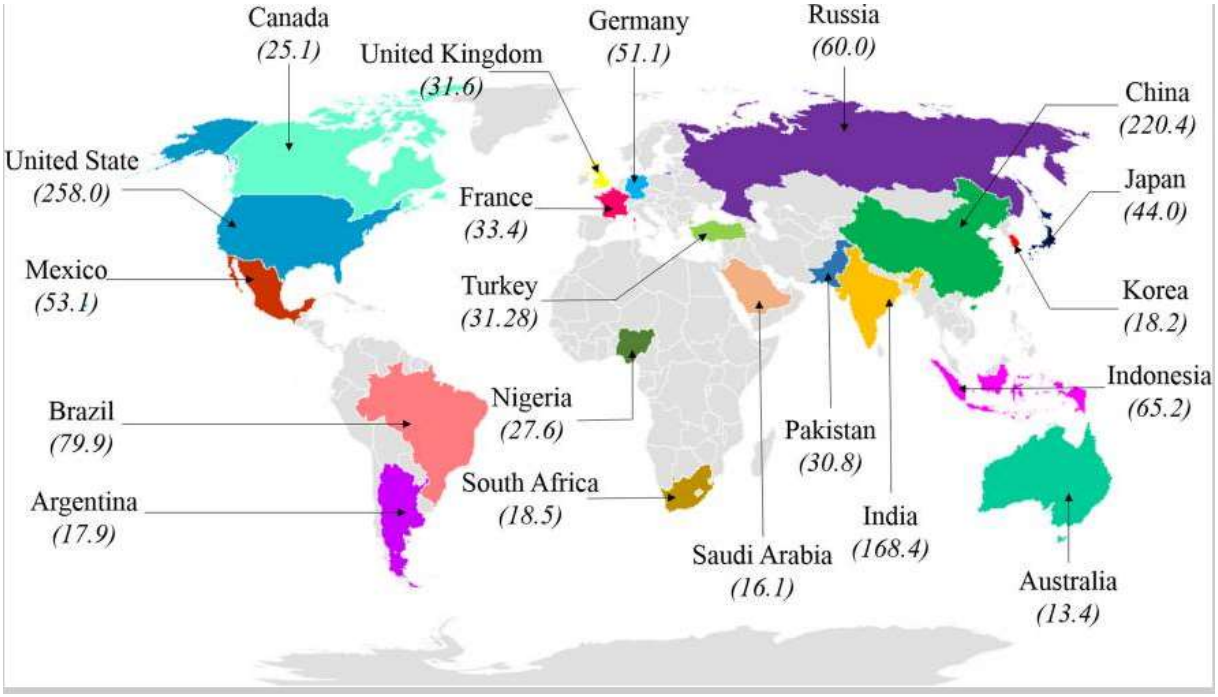

Figure 2 – 2018 Municipal solid waste outlook in million metric tonnes. [4]

1.2 STATE-OF-THE-ART – GAS ENGINES for OFC

Engine manufacturers are continuously developing modern Internal Combustion Engines for operation on renewable and cleaner fuels. Some of the recent efforts are based on pure Hydrogen gas for road vehicles and motorsport applications (e.g., Yamaha Hydrogen 5.0 V8) and multi-fuel strategy for heavy-duty vehicles and generators (e.g., Cummins fuel-agnostic engine platforms).

Figure 3 – Yamaha Hydrogen 5.0L V8 at left and Cummins X15H at right.

Internal combustion engines could be developed to employ different fuel-delivery and ignition strategies to optimize their use. Figure 4 presents the diversity of possibilities for pure hydrogen and their mixture with high H2 concentration. Fuel can be delivered via port fuel injection, direct injection, or even a combination of both, while ignition strategy will vary depending on fuel type and its properties, engine constructive technology, and range of applications. Multi-fuel engines present similar strategies as those presented in Figure 4 for pure Hydrogen.

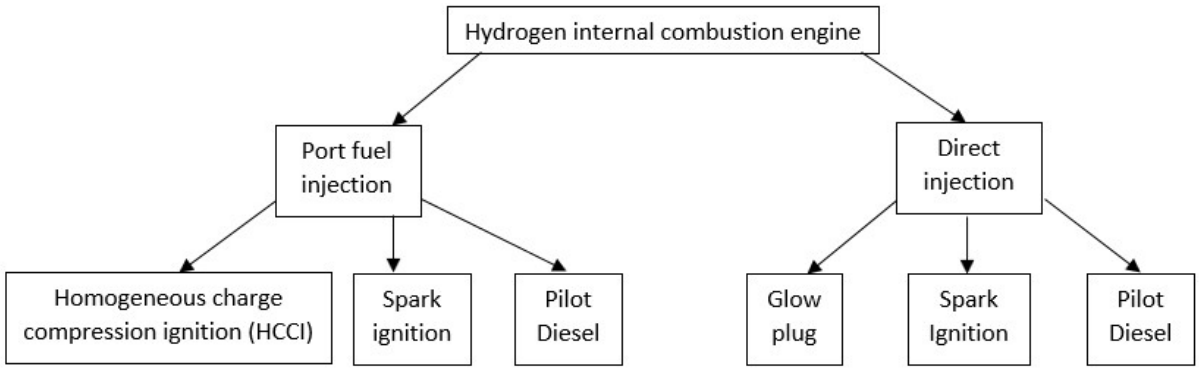

Figure 4 – Simplified diagram of injection and ignition strategies for Hydrogen internal combustion engines. Adapted from [5].

In terms of power generation, Internal Combustion Engines-Generators (ICEGs) still play a significant role in developing countries [6] due to their lower cost, larger availability, and better fuel flexibility [7] when compared to gas turbines [8]. In Brazil, gas engines have been the preferred technology for landfill gas utilization in WtE projects.

Table 1 – Gas turbine and gas engines main characteristics for power generation [9]

GAS TURBINES	RECIPROCATING ICE
High Combined Cycle efficiency	High Single Cycle efficiency
Low Emissions and noise	High part-load efficiency
Power density	Fast Start capabilities
CHP high temperature	CHP low temperature
Inertia	Multi-unit approach
H_2 capability	Better Fuel-flexibility
Higher cost	Lower cost

Advanced reciprocating engines are potential means of converting alternative fuels and synthesis gases into power [7], [8]. Compression Ignited (CI) engines tend to be the preferred technology over Spark Ignited (SI) [10]. Figure 5 shows a series of Wärtsila 20V24SG gas generator sets in operations in the UTE-LORM in Brazil. These engines can burn a broad range of gaseous fuels with thermal efficiency in excess of 40% in single cycle application. Overall fuel efficiency can be largely improved by means of combined power cycles utilization or heat and power systems.

Figure 5 – Wärtsila 20V24SG gas generator sets with a total combined output of 204 MW in thermoelectric powerplant UTE-LORM, located in State of Espírito Santo – Brazil.

Large gas engine power plants are potential candidates for the application of Carbon Capture and Storage (CCS) technology to reduce carbon dioxide (CO_2) emissions from fossil fuel power generation [11]. Carbon Capture and Storage (CCS) technology combined with more efficient power generation would further reduce CO_2 emissions [11]. Renewable energy

sources also play a major role to substitute fossil fuels in any combined strategy to decrease greenhouse gas emissions. In the Brazilian scenario, renewable fuels such as ethanol capture CO_2 naturally during sugar-cane plant growth, a process called carbon fixation; CO_2 capture could also occur in post-combustion [12] processes. NO_x emissions, though, claim specific treatment such as that based on catalytic converters.

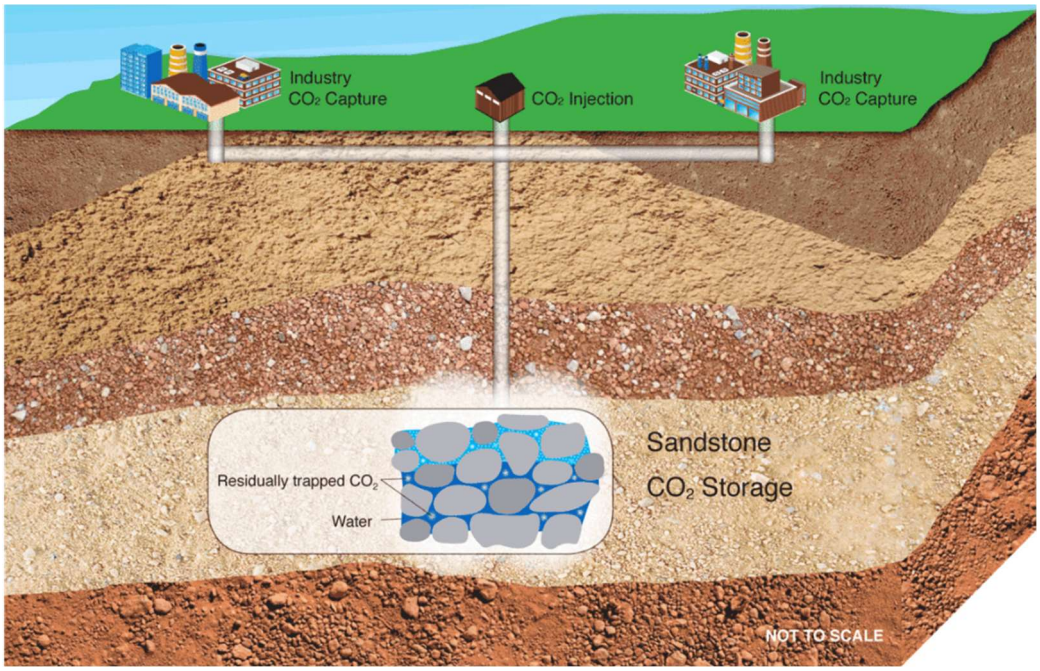

Figure 6 – Simplified diagram of carbon capture and underground storage [13].

There are three main technologies to promote carbon capture: pre-combustion, post-combustion, and oxyfuel combustion operations. Pre-combustion capture is composed of conversion systems that transform fuels into a mix of hydrogen gas and carbon dioxide. The principle consists of partially oxidizing fuel (e.g., coal) in oxygen/air and steam under high temperature and pressure to obtain synthetic gas (syngas). Syngas is a mixture of carbon monoxide (CO), carbon dioxide (CO_2), hydrogen (H_2), and smaller portions of methane (CH_4), and can undergo a process called water-gas shift reaction (WGSR) to produce a gaseous mixture comprising of H_2 and CO_2. After removing the CO_2, combustion takes place with H_2-rich fuel. Post-combustion carbon capture removes carbon dioxide from flue gas streams after fuel oxidation. This technology is the preferred option for retrofitting existing power plants, capable to recover CO_2 at a rate of up to 800 tons per day. [14]

Oxyfuel combustion takes place in an oxygen-enriched gas mix instead of air. Input air enters an Air Separation Unit where almost all of the Nitrogen is removed, yielding a stream of 95% higher oxygen concentration. This work deal with oxyfuel combustion of gaseous fuel extracted from the thermal degradation of Refused-Derived Fuel from MSW disposal centers.

A search on the *Science Direct* database using the keywords of the present research

showed the following result findings:

"Oxyfuel" – 2,925;

"Refuse derived fuel" – 16,178;

"CHP plants" – 23,463;

"Gas engine" – 210,760;

"Carbon Capture and Storage" – 138,592

By combining all of these keywords in the advanced search window (find articles with these terms) the system returns a list of null articles for that consultation. Therefore, the proposed research shows a good deal of novelty.

1.3 RESEARCH OBJECTIVES

Considering that few researchers have addressed the application of CCS technology in CHP plants based on the oxyfuel combustion in WtE projects, this work is mainly focused on presenting a mathematical model to predict relevant gas engine data from the burning pyrolysis gas from Refuse-Derived Fuels in oxyfuel mode. The main objectives of this work are:

- to develop a thermodynamic simulation code for oxyfuel combustion (OFC) analysis;
- to obtain engine performance parameters in different oxidizer composition;
- to promote basic engine analysis when experimental testing is complex, costly or not viable.

After these goals, the following secondary objectives fulfill the general purpose of the work:

- investigate the oxyfuel combustion applied to CHP plants;
- to conduct a feasibility study of CHP plants operating with RDF in oxyfuel combustion mode for Carbon Capture and Storage application.

1.4 OUTLINE

This work is structured in five chapters as follows:

Chapter 2 presents a literature overview regarding the most relevant concepts related to this study. It is divided into four sections:

- A brief historical background of oxyfuel process;
- Latest research on this theme;

- The mathematical model used in this work;
- How results were validated by comparing theoretical results with an actual engine.

Chapter 3 contains CHP feasibility study with all results of the different OFC modes gathered and calculated.

Chapter 4 presents an overview of a simulated application of this concept in Brasilia waste landfill

Chapter 5 contains the final remarks of this work along with the recommendations for future studies to improve results and address specific events observed during the current study.

Chapter 2

2 CONCEPTS

In this chapter, an overview of the most relevant concepts for the present study is given. First, a brief historical background of oxyfuel combustion is presented. Then, the second part deals with some of the latest and most relevant studies on OFC. The third part presents the mathematical and numerical models developed for this research, along with code validation.

2.1 OXYFUEL COMBUSTION

Oxyfuel combustion (OFC) consists in carrying out the combustion process removing the nitrogen from the oxidizer. The first application describing its implementation dates back to the beginning of the 20th century when French engineers Edmond Fouché and Charles Picard developed oxy-acetylene for welding purposes, and later for metal cutting.

OFC technology applied to reciprocating ICE is quite novel [15] and appears as one of the most promising solutions to eliminate pollutants while maintaining energy conversion efficiency and providing the expected carbon capture [16]. Oxyfuel combustion concept is not new and still there are few works available in the literature [2], [15] applied to gas engines in non-conventional fuels. With the removal of nitrogen from the oxidizer, combustion process may take place under oxygen-enriched conditions, using the exhaust gas recirculation (EGR) of CO_2 and water vapor to control the high combustion temperatures to prevent overheating issues [17]. Recycling flue gas is also a means to achieve lower flame temperatures in ICE's [18]. Equation 1 and 2 show the main products of air (conventional) and oxyfuel combustion of a generic hydrocarbon or alcohol.

$$C_xH_yO_z + a(O_2 + 3{,}76N_2) \rightarrow bCO_2 + cH_2O + dN_2 + eO_2 \quad (1)$$

$$C_xH_yO_z + a(O_2 + \beta CO_2) \rightarrow bCO_2 + cH_2O \quad (2)$$

Carbon capture is thus facilitated when performing oxyfuel combustion since the water in flue gases can be condensed leaving a stream of pure carbon dioxide. For combined cycle and cogeneration system, the combustion has to be performed in stoichiometric mode to avoid the presence of costly oxygen in the products of the reaction. It is also possible to note that nitrogen oxide emissions are eliminated once the combustion process occurs in the absence of nitrogen. Figure 7 illustrated the intake and exhaust strokes of an ICE operating in oxyfuel mode. OFC oxidizer is generally composed of pure oxygen mixed with recirculated flue gases. The reactant mixture comprised of oxygen, fuel and recirculated flue gases enters the engine during intake stroke, and products, mostly carbon dioxide and water, leaves the engine during exhaust stroke. Carbon dioxide can be stored or converted to carbon-based fuels through methods of electro-catalytic CO_2 transformation [15].

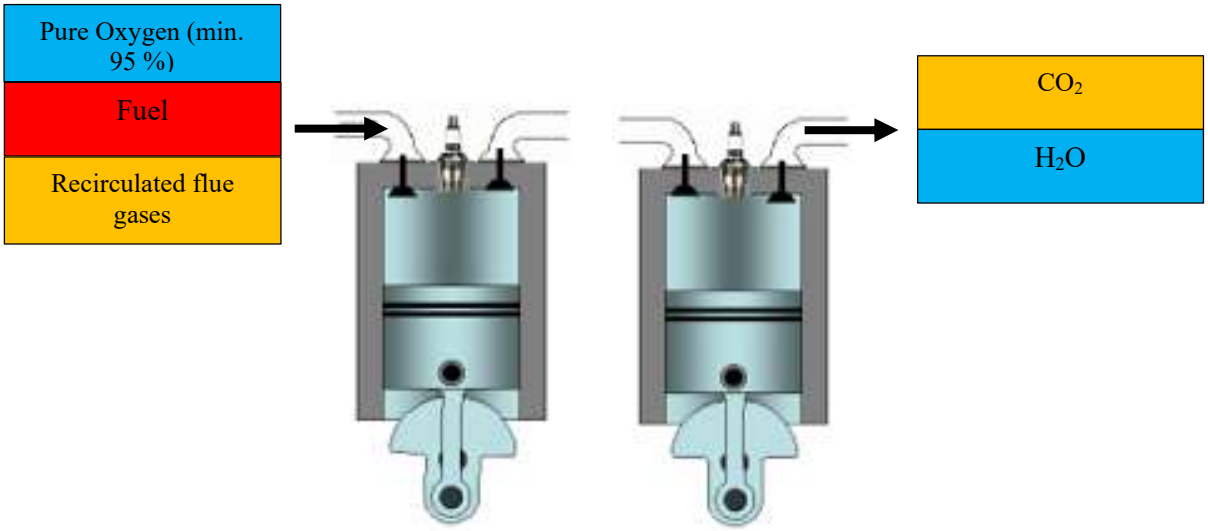

Figure 7 – Oxyfuel concept applied to reciprocating internal combustion engine.

2.2 RELATED RESEARCH

Serrano et al. [19] provided a theoretical and experimental evaluation of spark-ignition premixed oxyfuel for future CO_2 captive power plants. In that work, the authors stated that the engine should be operated in near-stoichiometric conditions. Another issue addressed referred to EGR dilution rates which ranged between 60% and 70% to avoid in-cylinder temperature excess after the compression stroke, to further avoid undesired knocking that could potentially lead to mechanical failure, and also to ensure combustion stability.

Wu et al. [20] applied water direct injection combined with oxyfuel to investigate its potential for thermal cycle efficiency improvements. Water was heated up through engine

coolant and exhaust gas before being injected into the cylinder. Waste heat was recovered, and, under appropriate test conditions, thermal efficiency increased from 33% to 53%.

Shudo et al. [21] evaluated the characteristics of the combustion and the exhaust emissions from a spark ignition engine fueled with several kinds of gases selected simulating pyrolysis products of shredder dust (WtE). In that study, fuels with heating values as low as 5.02 MJ/m³ were successfully used in internal combustion engines. Another remark was that waste-pyrolysis gases containing a large amount of inert gas emitted low NO_x in lean combustion mode ($\lambda = 1.5$).

Fiore et al. [22] reviewed the use of residual forest activities or wastes from the agricultural industry for power and heat generation to supply energy to peripheral areas with minimum pollutant emissions. The work addressed a broad range of technologies, such as, dual-fuel compression ignition engines, homogeneous charge spark ignition engines and direct injection spark ignition engines under syngas operating conditions from both experimental and numerical points of views. The performance and the emissions of the engines were examined and discussed showing that syngas composition was the most important parameter for the performance of different engines.

German company Spanner Re² GmbH developed CO_2-neutral biomass power plants across Europe, in ranges from 500 kW to 2 MW. In Latvia, a cascade of 20 engines burns syngas obtained from the thermal gasification of dry wood for heat and power applications (Fig. 8)

Figure 8 – Spanner Re² GmbH CHP plant located in Valka, Latvia.

The use of fuel gases from renewable sources is a promising technology for heat and power generation at near zero carbon emissions. The large-scale implementation of such technologies, including renewable hydrogen, will take time. Oxyfuel combustion of gaseous

fuel obtained from thermal conversion of carbon-based energy feedstocks, either by pyrolysis or gasification, is a promising intermediate technology towards a hydrogen-based power production economy.

2.3 MATHEMATICAL and NUMERICAL MODEL

The proposed model is based on an energy balance applied to the main processes of the engine in which the indicated efficiency (η_{ind}) is obtained after inferring cycle losses from intake work (ε_{inw}), heat transfer to the walls (ε_{wht}), and exhaust gases energy (ε_{exh}) as defined by Martin [23]. It will be shown later in the chapter that the indicated efficiency helps define effective efficiency (η_e) once mechanical efficiency (η_{mec}), which tracks the cylinder friction losses, is calculated. Therefore, all the relevant engine losses are taking into consideration in Eq. (3). As such, the model can be referred as a Global Energy Balance Model (GEBM) given by

$$\eta_{ind} + \varepsilon_{wht} + \varepsilon_{exh} + \varepsilon_{inw} = 1 \tag{3}$$

Figure 9 illustrates the main processes along the Otto cycle in a temperature versus entropy chart.

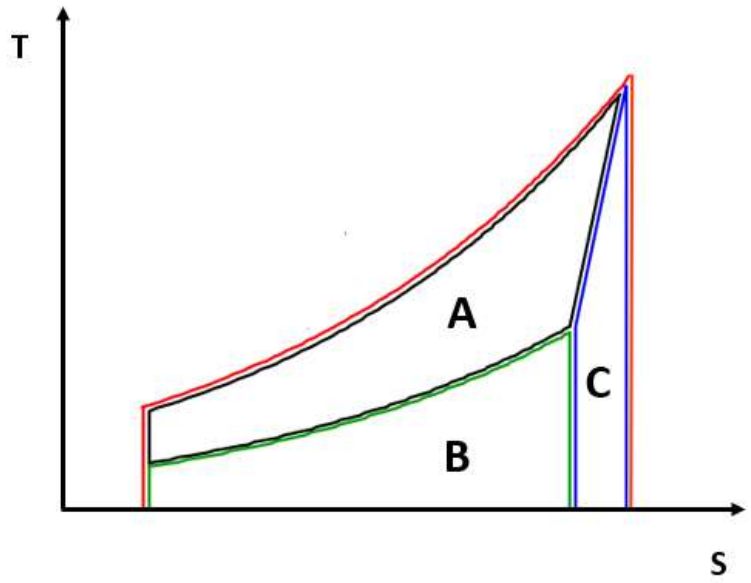

Figure 9 – Temperature-Entropy (T-S) diagram of an Ideal Otto Cycle [23].

Theoretical four stroke naturally aspirated Otto Cycle can be inferred by the following areas:

- The total area A+B+C under red contour is the heat supplied to the engine (η_i);

- Area A corresponds to the ideal work delivery by the engine, without considering the intake work losses;
- Area B corresponds to rejected heat during exhaust stroke (ε_{exh});
- The C area corresponds to heat loss due to engine cooling during power stroke expansion (ε_{wht}).

The terms in Eq. (3) are non-dimensional and are obtained after dividing a given thermodynamic process area (A_i) by the total area (heat addition $=\sum A_i$), such that $\varepsilon_{exh} = A_B/A_{(A+B+C)}$, $\varepsilon_{wht} = A_C/A_{(A+B+C)}$ and $\eta_i = A_A/A_{(A+B+C)}$. The internal engine efficiency (η_i) needs further formulation to include the intake stroke work relation (ε_{inw}) giving by the green area in Fig. 10. The engine net work (indicated power) is given by the balance between the relative power stroke (η_i) and the relative intake work (ε_{inw}) such that $\eta_{ind} = \eta_i - \varepsilon_{inw}$.

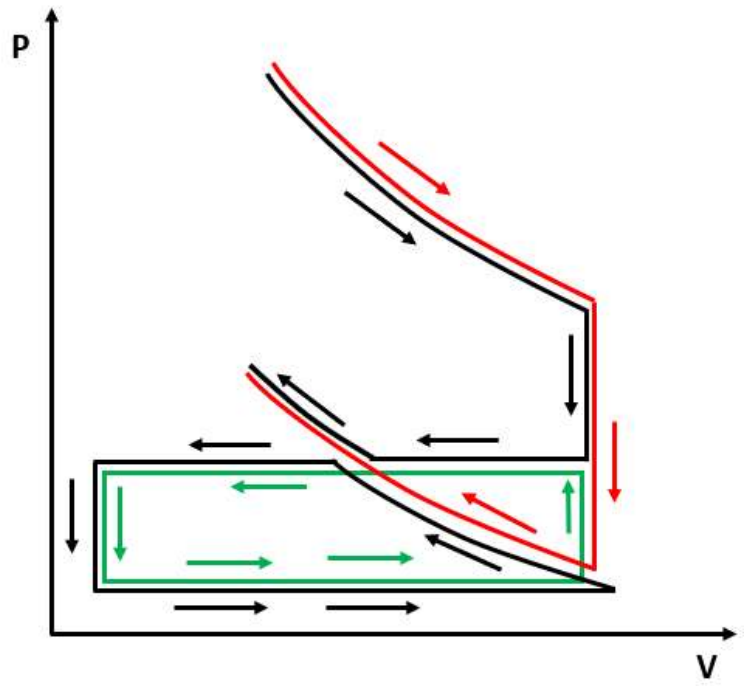

Figure 10 – Intake breathing work (green line) in Pressure-Volume (P-V) diagram of an ideal Otto cycle [23].

Figure 11 shows a turbocharged Otto Cycle in the T-S diagram. While compression stroke is still the same from 1 to 2, as well as heat release from 2 to 3, the end of power stroke must be altered to allow the flue gases to flow through the exhaust valve (4-5*) and run the turbine (5-6). Therefore, engine exhaust must take place at higher pressure (p_4). Since the turbine expansion process is not reversible, some entropy is generated between 5-6. Entropy is also generated when the flue gases exit the cylinder engine. Process 5* to 5 refers the flue gas

cooling along the exhaust pipe. On compressor side, intake occurs at ambient pressure (p_0) and temperature (T_0), from t stage "0". Compressor then raises, non-isentropically, air pressure to state 1*. Then, intercooling reduces the temperature of the pressurized air to T_1, prior to the compression stroke 1-2.

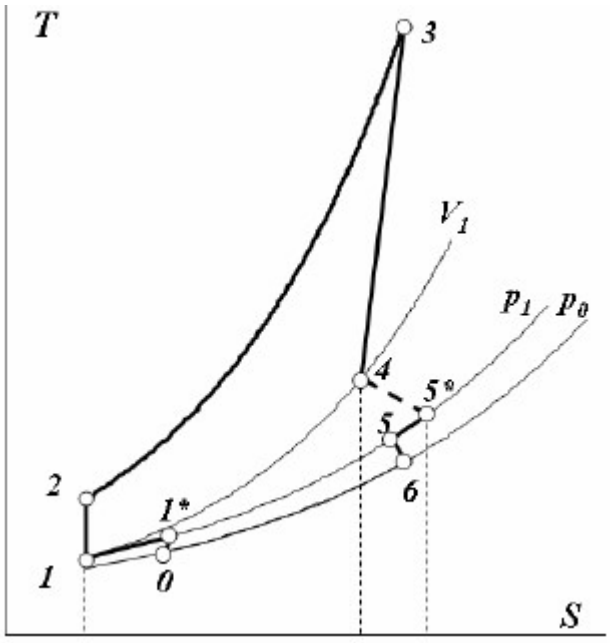

Figure 11 – Temperature-Entropy (T-S) diagram of a turbocharged Otto Cycle [23].

An overview of the model is displayed in Figure 12. Since the GEBM model does not give the thermodynamic states along the cycle, an auxiliary simplified model was also developed to overcome such constraint. For combined heat and power applications the engine exhaust temperature is a necessary information for process heating. Exhaust temperature can be inferred by the energy content in the flue gases, from the GEBM model or by an auxiliary model that provides the thermodynamic properties stated along the cycle. This simplified model helps to validate the GEBM model results and set the limits for the thermodynamic properties along the cycle.

As it can be seen from Fig. 12, the model can handle a broad range of conventional Otto-cycle fuels, and others, such as landfill gas, biogas, syngas, pyrolysis gas, natural gas, etc.

As for the oxidizer, the model is able to deal with conventional air combustion (lean and stoichiometric) and oxyfuel applications in a broad range of oxygen dilution by carbon dioxide and water. In this work the relative mass proportion of oxidizer were 75% CO_2 and 25% O_2 (75/25), 80% CO_2 and 20% O_2 (80/20), 85% CO_2 and 15% O_2 (85/15). In addition to the reactants, the model also need data from the geometric and operating engine conditions, such as compression and equivalence ratios, engine *rpm*, and so on, as depicted in Fig. 12.

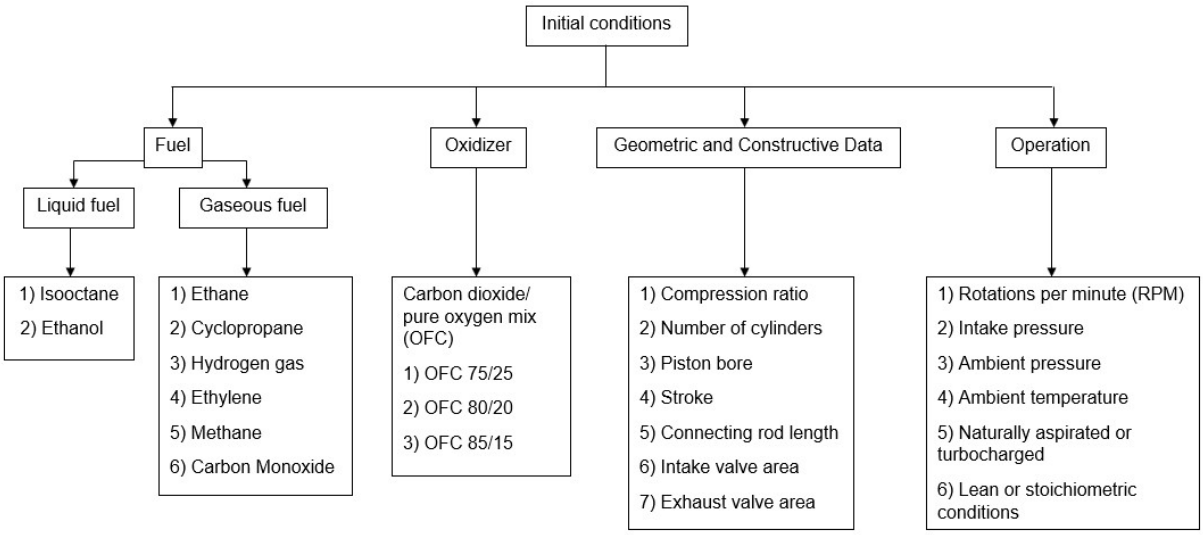

Figure 12 – Diagram of modelling conditions in Engineering Equation Solver software.

The terms in Eq. (1) are obtained by modeling the processes interactions during the cycle [23]. Engine cooling losses through the walls, as function of charging coefficient (r), mean piston speed (w), cylinder diameter (D) and compression ratio (χ), are calculated from

$$\varepsilon_{wht} = 0.015(rwD)^{-0,2}(\chi^{0,8} + 3\,\chi^{-0,4}) \tag{4}$$

The charging coefficient (r) is given by

$$r = \left(\eta_{isc}\eta_{isT}\frac{\dot{m}_{eg}h_{inT}}{\dot{m}_{Air}h_{inAir}}\right)^{\frac{\gamma}{\gamma-1}}\frac{T_{inAir}}{T_{outAir}} \tag{5}$$

For gaseous fuels, intake losses ε_R, as a function of pressure difference between intake and exhaust (ΔP_{inw}), the charging coefficient (r), the volumetric stoichiometric ratio (V_{a1}), the equivalence ratio (ϕ), the mixture density (ρ_0), the fuel lower heating value (LHV) and the volumetric stoichiometric ratio (m_{a1}). The losses are computed by

$$\varepsilon_{inw} = \frac{\Delta P_{inw}}{r\rho_0\left(\frac{V_{a1}}{V_{a1}+\phi}\right)\phi\frac{LHV}{m_{a1}}} \tag{6}$$

where ΔP_{inw} the difference between exhaust and intake pressures is given by

$$\Delta P_{inw} = P_4 - P_1 \tag{7}$$

Losses from the exhaust are calculated by

$$\varepsilon_{exh} = \frac{1}{\chi^{\xi}} - \varepsilon_P \left(\frac{2}{\chi^{\xi}+1}\right) \tag{8}$$

Where the convenience factor ξ is obtained by the following equation

$$\xi = -\frac{\log(1-\eta_{th})}{\log(\chi)} \tag{9}$$

For $0 \leq \varepsilon_R \leq 0.015$

$$\xi = 0.277 + 0.06(1-\phi + (1-0.1\chi^{0.5})(1-\phi)^{2,5}) \tag{10}$$

The effective power is given by the brake mean effective pressure ($\bar{p}_e$) and engine geometric (V_c), design (N) and operating regime (rpm) using

$$P_e = \bar{p}_e V_c \frac{rpm}{N} \tag{11}$$

The brake mean effective pressure is given by

$$\bar{p}_e = \eta_e r \rho_0 \frac{AFR_{vb}}{(AFR_{vb}+\phi)} \frac{\phi LHV}{AFR_{mb}} \tag{12}$$

In Eq. (12), η_e is the engine brake efficiency, air to fuel ratio in volumetric (AFR_{vb}) and mass basis (AFR_{mb}).

To complete the terms in Eq. (3) it is necessary to infer the engine indicated efficiency (η_{ind}), related to the mechanical (η_{mec}) and effective counterparts, given by

$$\eta_e = \eta_{mec}\eta_{ind} \tag{13}$$

Engine mechanical efficiency is inferred by

$$\eta_{mec} = 1 - \frac{\bar{p}_f}{\bar{p}_i} \tag{14}$$

In Eq. (15), $\bar{p}_f$ is the engine mean friction pressure and $\bar{p}_i$ is the mean indicated pressure. Engine mean friction pressure is obtained from

$$\bar{p}_f = \bar{p}_{f,0} + k_s(2\bar{p}_c + \bar{p}_i)k_w \frac{w}{D} \tag{15}$$

$$\bar{p}_i = \eta_{ind} r \rho_0 \frac{AFR_{vb}}{(AFR_{vb} + \phi)} \frac{\phi LHV}{AFR_{mb}} \tag{16}$$

In four stroke engines used as generators, $\bar{p}_{f_0} = 70\ kPa$, $k_s = 0{,}02\ kPa$, $k_w = 0{,}70\ kPa$, $\bar{p}_c = 700\ kPa$. [23]

Brake specific fuel consumption is given by

$$SFC = \frac{1}{\eta_e LHV} \tag{17}$$

The auxiliary model, referred as State Thermodynamic Model (STM) calculates the thermodynamic properties along the ideal Otto cycle. It is helpful in characterizing the limits of the main thermodynamic properties, such as temperature and pressure.

First, the stoichiometric equation for a given fuel and oxidizer composition is calculated using the oxyfuel combustion reaction presented in Eq. (2).

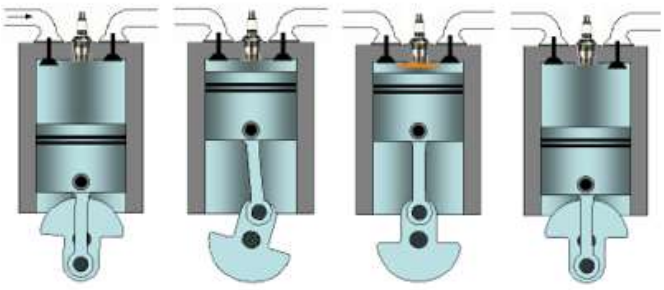

Figure 13 – From left to right: thermodynamic states 1, 2, 3 and 4 of an Ideal Otto cycle, corresponding to those shown in the Fig 7. [24]

The main equations of the STM model follows that for a four stroke Otto Cycle. Cylinder and engine total displacement are calculated by

$$V_{cyl} = \frac{\pi D^2 h}{4} \tag{18}$$

$$V_{eng} = V_{cyl} \cdot n_{cyl} \tag{19}$$

Compression ratio is given by

$$\chi = \frac{V_1}{V_2} \tag{20}$$

Where V_1 is the volume (displacement) at the bottom dead center, while V_2 is that at top dead center.

The code was developed to deal a broad range of fuels such as syngas, pyrolysis gas, landfill gas, gasoline, ethanol and a mix of those. Fuel composition, therefore, must be given in terms of volume of mass fraction. Carbon dioxide may also appear as a component in the fuel gas, when pyrolysis and gasification are executed in carbonaceous energy feedstocks.

In this case, CO_2 in flue gases may be from exhaust recirculation, carbon oxidation or the fuel itself (reactant). Oxidizer mass compositions in the reactant mixture, in kg, are calculated using equations 21 to 23, for oxyfuel, oxy-enriched and conventional combustion processes in the ICE.

$$m_{CO2}^r = (n_{CO2} + \beta n_{AF_{stoic}}) MW_{CO2} \tag{21}$$

$$m_{N2}^r = (n_{N2} + n_{AF_{stoic}} \Gamma) MW_{N2} \tag{22}$$

$$m_{O2}^r = n_{AF_{stoic}} MW_{O2} \tag{23}$$

$$m_{stoic}^{oxi} = n_{AF_{stoic}} (\beta + \alpha + 1) \tag{24}$$

In conventional air combustion, $\alpha = 3{,}76$ since this is the nitrogen mole fraction in atmospheric air, and $\alpha = 0$ for CO_2 and O_2 oxidizer mix. In oxyfuel application, the CO_2 concentration in the oxidizer mix is given by the parameter β, with $\alpha = 0$. In fact, the oxygen separation unit is not 100% efficient and some traces of nitrogen can be found in the oxygen

stream.

Considering a steady-state condition typical of electric generators powered by ICE, equivalence ratio ϕ is always equal to or less than one. STM code then returns the key thermodynamic properties of products in states 3 and 4, from a given fuel and oxidizer mix input (states 1 and 2). The system equivalence ratio is given by

$$\phi = \frac{AF_{act}}{AF_{stoic}} \tag{25}$$

where stoichiometric air to fuel ratio is that when no traces of fuel and oxidizer can be found in the products of the combustion and is given by

$$AF_{stoic} = \left(\frac{m_{oxi}}{m_{fuel}}\right)_{stoic} \tag{26}$$

The actual air to fuel ratio is given by

$$AF_{act} = \frac{m_{oxi}}{m_{fuel}} \tag{27}$$

In the simulated case of oxyfuel combustion, the reaction is performed in stoichiometric conditions, therefore, total mass of the reactant mixture is given by

$$m_{total}^{r} = m_{stoic}^{fuel} + m_{stoic}^{oxi} \tag{28}$$

The entire code underwent a thorough mass conservation check based on chemical balance between reactants and products. The products of stoichiometric combustion, using air or pure oxygen as oxidizer, were calculated after balancing carbon (C), hydrogen (H), oxygen ($O_)$, and nitrogen (N) among reactants and products. The code then returns the products (CO_2, H_2O, N_2) of the stoichiometric combustion. The mass of any product species is calculated using

$$m_i^p = n_i^p MW_i \tag{29}$$

Total mass of the products of the reaction, neglecting minor species, is given by

$$m^p = m_{CO2}^p + m_{H2O}^p + m_{N2}^p \tag{30}$$

Products of lean combustion are calculated in similar manner, but including oxygen in flue gases' parcel.

The program was designed to compute the four thermodynamic states of the theoretical Otto Cycle. First state consists to that at the end of the mixture intake, prior to the compression at 180 degrees of crankshaft. Intake volume at BDC, state 1, is given by Eq. (4).

For a given temperature, pressure and volume, the ideal gas returns the number of moles of the mixture (n_1) that fill the entire cylinder after intake stroke.

$$P_1 V_1 = n_1 R_u T_1 \tag{31}$$

The code returns other key thermodynamic properties such as specific heats of the reactants, defined by the following equations

$$c_p^1 = \sum Y_i \, c_{p,i}(T_1) \tag{32}$$

$$c_v^1 = \sum Y_i \, c_{v,i}(T_1) \tag{33}$$

The ratio of specific heats that gives polytropic coefficient for the adiabatic compression and expansion processes is readily obtained from

$$\gamma(T_1) = \frac{c_p(T_1)}{c_v(T_1)} \tag{34}$$

It is important to remind that CO_2 and H_2O are the only products of the stoichiometric hydrocarbon combustion. Therefore, the ratio of specific heat of the mixture is strongly dependent on temperature, thus influencing engine's overall efficiency.

Internal energy of the thermodynamic system at state 1 is given by

$$U_1 = \sum m_i \, u_i(T_1) \tag{35}$$

Properties at second thermodynamic state, at the end of compression stroke (TDC) must be inferred after applying conservation of energy for the process, thus

$$Q_{12} + W_{12} = U_2 - U_1 \tag{36}$$

For an adiabatic compression ($Q_{12} = 0{,}0$), adiabatic compression work is obtained from

$$W_{12} = \frac{R}{(\bar{\gamma}_{12} - 1)}(T_2 - T_1) \tag{37}$$

In Eq. (36), the ratio of specific heats is averaged between thermodynamic states 1 and 2. Temperature at the end of the process is obtained from the following relation

$$P_1 V_1^{\bar{\gamma}_{12}} = P_2 V_2^{\bar{\gamma}_{12}} \tag{38}$$

In combination with the ideal gas law

$$P_2 v_2 = RT_2 \tag{39}$$

With two independent properties determined, thus characterizing the thermodynamic state, the code may provide all the remaining thermodynamic properties.

Third thermodynamic state occurs at TDC following the combustion reaction at constant volume. This state is determined by considering no work transfer along the process. Heat added to the system is equivalent to the enthalpy of reaction of the mixture.

Based on stoichiometric relations the code returns fraction of oxyfuel combustion products (CO_2, H_2O) and other properties at state 3.

$$Y_{O_2}^a = \frac{m_{O_2}^a}{m_a} = 0 \tag{40}$$

$$U_3 = \sum m_i \, u_i(T_3) \tag{41}$$

Since the volume at the end of volumetric expansion is equivalent to that prior to compression, then

$$V_4 = V_1 \tag{42}$$

First law applied to expansion process (power stroke) 3 to 4 is given by

$$Q_{34} + W_{34} = U_3 - U_4 \tag{43}$$

$Q_{34} = 0.0$ since this process is adiabatic with the following *PV* relation

$$P_3 V_3^{\bar{\gamma}_{34}} = P_4 V_4^{\bar{\gamma}_{34}} \tag{44}$$

where the expansion work is inferred by

$$W_{34} = \frac{R}{(\bar{\gamma}_{34} - 1)}(T_3 - T_4) \tag{45}$$

Temperature T_4 was calculated using ideal gas law. As a result, state properties for the end of compression are obtained.

$$P_4 v_4 = RT_4 \tag{46}$$

The GEBM and STM models comprised of 45 equations were implemented in the Engineering Equation Platform (EES), for prediction analysis. EES is an equation-solving program able to integrate thousands of coupled non-linear algebraic and differential equations. It also incorporates a high-accuracy thermodynamic and transport property database for a large number of chemical species. Additional equations related to the thermodynamic state of gases are obtained from the NASA polynomials (ideal gases) stored in the internal function library of the EES platform. For numerical integration, EES applied a variant of the trapezoid rule along with a predictor-corrector algorithm. In EES, iteration stops when the relative residual of a variable is less than 1.0E-6, or the change in variables during successive iterations is reduced below 1.0E-9.

2.4 VALIDATION

The GEBM was validated comparing data of actual engine generator for a given operating condition. Table 2 lists main engine characteristics and operating conditions.

Validation results were obtained by inserting in EES simulation platform the technical data from a single unit 2 MW Caterpillar G3520E [26] generator set and corresponding catalog reference information. Some of the engine's data used as inputs into EES software are presented in Table 2, while the complete datasheet is located in the Appendix section of this work.

Table 2 – Some engine data used in GEBM simulation and validation.

PARAMETERS	INPUT
Engine speed	1500 rpm
Compression ratio	11.9:1
Fuel	Natural Gas
Fuel flow	509 Nm^3/h
Piston Bore	170 mm
Crankshaft Stroke	190 mm
Total engine displacement	86 L

Table 3 presents the numerical predictions and the performance data of the G3520 engine. It could be noted that similar results were obtained for natural gas fuel operating at equivalence ratio $\phi = 0.57$ and for conventional air combustion (CAC) when compared with data from the manufacturer's datasheet. The code slightly underestimated engine thermal efficiency by less than 3 pp. Numerical predictions deviation from the G3520 engine for specific fuel consumption, power output, heat rejection, and exhaust gas temperature are less than 15%.

The proposed model is capable of reproducing with good level of confidence basic operating conditions of an actual engine. Therefore, relevant engine data can be obtained for combined heat and power assessments. The model was then applied for oxyfuel combustion scenarios, the main purpose of this dissertation.

Table 3 – Code validation

PARAMETER	GEBM ϕ=0.57	G3520 ϕ=0.57
Thermal efficiency (%)	42.4	45.3
Exhaust gas temperature (°C)	496	430
SFC (g/kWh)	250	251
Exhaust heat rejection (kW)	1682	1462
Power output (kW)	2085	2100

Table 4 shows some of data obtained from the three OFC scenarios for the Caterpillar G3520E engine using both GEBM and STM models.

Table 4 – Gas engine oxyfuel simulations for natural gas.

	OFC 75/25		OFC 80/20		OFC 85/15	
Parameter	GEBM	STM	GEBM	STM	GEBM	STM
Thermal efficiency - η_e (%)	43.2	46.1	42.7	46.1	42.1	46.2
T_{exh} (K)	1119	1026	968	970	804	1016
Engine power output (kW)	2217	2441	2200	2196	2172	1770
SFC (g/kWh)	227	228	222	228	231	228

It can be noted that the STM model yields higher thermal efficiencies (η_e) when compared to GEBM predictions. Thus, from a thermal efficiency standpoint, GEBM model is somehow conservative when compared to the STM model. The expected thermal effciency of the G3520E engine is above 45%. Therefore, the STM model over predicts this parameter while the GEBM model underestimated the performance of the engine. However, the STM model is almost insensitive to the oxidizer composition. Such drawback was not observed for the GEBM model. Exhaust gas temperature predictions for both models are somehow comparable, except for the 85/15 scenario. For 80/20, the difference between the results from the models is negligible. For OFC 75/25 oxidizer composition the deviation was of about 8% increasing to about 26% for OFC 85/15. This situation is the same for power output, where 80/20 presented near identical results for both GEBM and STM models. Power output is 10% higher for STM in OFC 75/25, while is 20% lower for 85/15 case. Despite those differences, brake specific fuel consumption could be approached by either model considering the highest variation was less than 2.5%. Therefore, for oxyfuel applications the GEBM model seems a better and appropriate tool for CHP studies under Carbon Capture and Storage technology.

Chapter 3

3 CHP STUDY

As previously mentioned, this study is a follow-up to the design of a combined heat and power (CHP) plant operating with Refuse Derived Fuels (RDF) under oxyfuel combustion mode. More specifically, it aims to evaluate the viability of this technology when CHP plant is based on Internal Combustion Engine Generators (gas engines).

This chapter is divided into three sections. First it is presented the proposed Combined Heat and Power Plant for the combustion of pyrolysis gas from RDF. Then, an overview of the three oxyfuel cases is shown and evaluated. A feasibility analysis is carried out with results from the three proposed oxidizer mixture composition (OFC's)

3.1 COMBINED HEAT AND POWER PLANT

Waste management is a major concern in environmental policies around the world. The concept in this work presents a route to use Refuse Derived Fuel in Combined Heat and Power plant with near-zero carbon dioxide emissions.

Figure 14 – From left to right: waste plant treatment in Brazil, picture from São Paulo City Hall. At the center, processed waste batch. At right, hand-size RDF fuel pellets.

Municipal solid waste generally termed trash or garbage represents an unwanted item constantly supplied by humans, being a continuous challenge due to expanding population. The combustible substance pretreated waste parcel is called Refuse-derived fuel, composed of 50% to 80% plastic and paper, while the remaining fractions are contributed by organics, wood, and textile [4]. Waste is separated, screened, and subsequently undergoing a drying process before

reaching a pelletizing machine, or other mechanical transformation.

Figure 15 presents a simplified diagram of the proposed Combined Heat and Power (CHP) plant. The main fuel byproduct is the pyrolysis gas to feed the power engine generators. The remaining yields such as char and bio-oil can be further employed for energy transformation or as a feedstock for the chemical industry, for instance.

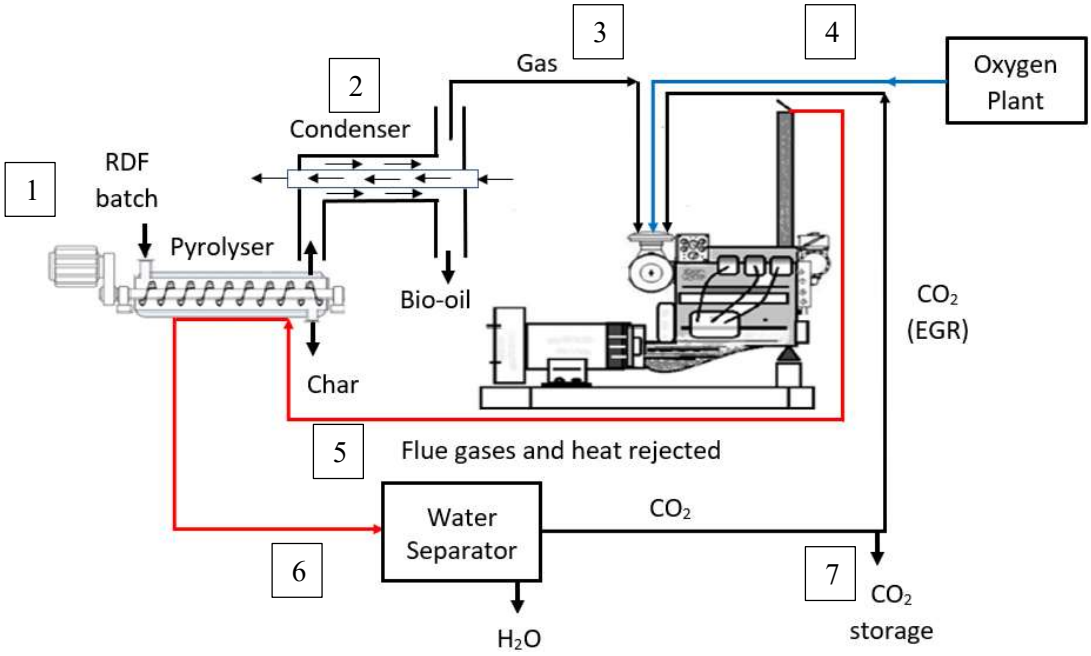

Figure 15 – Simplified diagram of proposed Oxyfuel CHP plant.

The processes displayed in Fig. 15 are:

1) Refuse Derived Fuel enters the screw pyrolysis reactor yielding char, and high temperature gas;
2) The gas mix moves to a condenser where it separates into a high-quality pyrolysis gas and bio-oil;
3) Pyrolysis gas is sent to the engine's intake to be further mixed with the oxidizer composed of carbon dioxide and pure oxygen from an oxygen separation plant;
5) Flue gas is transported to the pyrolysis reactor to sustain the RDF thermal degradation;
6) After passing through the pyrolysis reactor, flue gases enter a water condensation unit in which CO2 is separated to be further storage;
7) Part of the carbon dioxide is stored underground while the remaining share is directed to the engine's intake (exhaust gas recirculation).

The proposed CHP plant is feasible if RDF pyrolysis can be attained considering flue gas energy content as well as the temperature level that exits the gas engine. Table 9 will further presents that the predicted exhaust gas temperature from the GEBM model is in the range of 512 to 799 °C, therefore, suitable for RDF pyrolysis [27].

3.2 OFC SIMULATIONS

According to Rayca et. al. [27] gas from RDF has a calorific value between 15 and 30 MJ/Nm³, appropriate for OFC technology in terms of energy density and composition. The pyrolysis gas obtained from RDF is a mix of varying concentrations of CO, CO_2, CH_4, H_2, and other minor constituents. The mathematical model presented in Chapter 2 allows the user to simulate oxyfuel combustion with different fuel composition. The main fuel composition simulated in this work and the lower heating value of pyrolysis gas composition are presented in Table 5.

Table 5 – Pyrolysis gas composition (RDF) – main species concentration (%) [27].

Main species concentration	Concentration (% v/v)
CO	29,67
CH_4	11,67
C_2H_4	5,177
H_2	12,37
CO_2	2,821
C_3H_6	1,75
C_2H_6	1,399
N_2	35,143
LHV	13666 kJ/kg

It must be noted that pure oxygen should not be wasted in combustion process, considering the associated cost to its production. Therefore, the oxyfuel combustion must take place at stoichiometric condition [19]. For proper comparison, the burning regimes are set stoichiometric, for oxyfuel (OFC) and conventional air combustion (CAC). Table 6 presents oxidizer composition, in mass base, for both combustion modes.

Table 6 – OFC simulated cases composition and conventional air combustion

OFC		CAC	
CO_2	O_2	N_2	O_2
75/80/85	25/20/15	75.5	23.5

Table 7 lists main input data for the models. The four stroke turbocharged engine running with pyrolysis gas with a compression ratio of 11.9/1. Once characterized, the main parameters to infer engine cooling and friction losses are provided. Also, the necessary data to calculate engine intake losses are given along with the main operation conditions.

Table 7 – Major input data in Engineering Equation Solver software.

Input data	
pmf_0 for 4 stroke engines [23]	70 [kPa]
k_c for 4 stroke engines [23]	0.02
k_w for 4 stroke engines [23]	0,4 [kPa-s]
T_{fuel}	300 [K]
P_{fuel}	1.0 [bar]
T_{ref}	288 [K]
Compression ratio (χ) [26]	11.9/1
Piston mean speed (w)	9,5 [m/s]
Engine speed (rpm) [26]	1.500
Piston bore (D) [26]	0,170 [m]
Atmospheric pressure (P)	1.0 [bar]
Oxidizer temperature (T)	273 [K]
Turbocharger pressure [26]	3.92 [bar]
ϕ (equivalence ratio)	1.0
Engine net power	2.1 MW

Table 8 details the reactant and product composition for stoichiometric oxyfuel and conventional air combustion for 200 MW engine set with properties presented in Table 6.

For each of the simulated scenarios, oxidizer mass flow increases as oxygen dilution increases. The amount of oxidizer for oxyfuel combustion is larger compared to that for conventional air combustion. The latter claims 535,913 kg/h of air, while 631,140 kg/h is needed for OFC 75/25 oxyfuel combustion mode.

Table 8 – Main constituents of the OFC and CAC burning modes for a for 200 MW power plant.

	OFC 75/25	OFC 80/20	OFC 85/15	CAC
Intake oxidizer mass flow (kg/h)	631,140	800,264	1,082,474	536,913
CO_2 (intake kg/h)	507,991	677,146	959,349	-
O_2 (intake kg/h)	123,149	123,117	123,125	125,148
N_2 (intake kg/h)	52,024	52,024	52,024	411765
Fuel mass (intake kg/h)	127,500	127,500	127,500	127,500
Exhaust mass flow (kg/h)	758,640	927,764	1,209,974	664,413
CO_2 (exhaust kg/h)	647,114	816,458	1,099,000	139,063
CO_2 (exhaust %)	85.29	88	90.8	20.9
H_2O (exhaust %)	6.98	5.7	4.3	17.1
N_2 (exhaust %)	7.73	6.3	4.9	61,9
CO_2 captured (kg/h)	139,123	139,312	139,651	0,0

The very small concentration of nitrogen in oxyfuel mode occurs due to the process of oxygen extraction from air, which is not 100% accomplished. The high concentration of carbon dioxide in flue gas after oxyfuel combustion is appropriate for carbon capture and storage application. For instance, in OFC 75/25 prediction, 139,123 kg/h out of 647,114 kg/h in exhaust gas can be captured and sent to storage. A great majority is recirculated to allow the oxyfuel combustion process. Similar figures are observed for OFC 80/20 and OFC 85/15.

Figure 16 shows the recirculated mass flow of carbon dioxide and that in the flue gas from oxyfuel combustion mode. The mass flow varies from about 507,991 to 959,349 kg/h. The mass flow of CO2 in the exhaust gas varies from 647,114 to 1,099000 kg/h. The difference is the amount that is needed to be captured and stored, as depicted in Fig. 16. Yearly, the CHP-CCS plant would capture bear 1.1 million tons of CO_2.

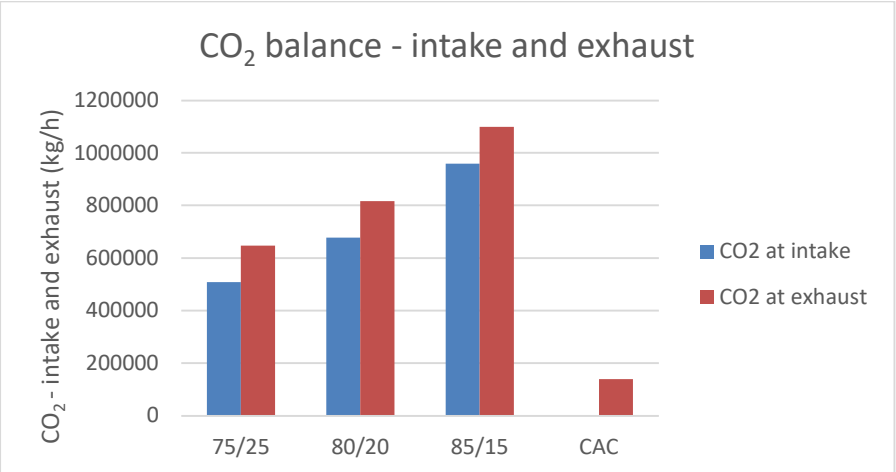

Figure 16 – Carbon dioxide mass flow balance for the simulated OFC conditions.

For OFC 75/25, 80/20 and 85/15, 85.29%, 88% and 90.8% respectively of exhaust emissions correspond to carbon dioxide that will be further stored underground. Carbon dioxide generated during the combustion for each case is around 139,000 kg/h. Based on these figures, the CO2 emission factor for all OFC combustion modes and conventional air combustion is about 690 g/kWh which is slightly higher than that from a natural gas open cycle power plant (~500 g/kWh).

Of great relevance is the mass flow of oxygen for the oxyfuel mode of combustion. The oxygen mass flow is at the order of 123,149 kg/h for a combined generator set with a total output of near 200 MW engine. Therefore, the specific oxygen consumption is about 615 g/kWh. The energy claimed by the oxygen separation plant varies from 0.1 to 0.3 MWh/ton of O_2 generated. The overall thermal efficiency of the plant will be reduced accordingly.

For the same power input and engine operational conditions, slightly differences in exhaust gas concentrations of H_2O and CO_2 were observed by varying the oxidizer composition in OFC mode, as presented in Table 8.

Table 9 – Numerical predictions for OFC and CAC burning modes in stoichiometric conditions.

	OFC 75/25	OFC 80/20	OFC 85/15	CAC
Exhaust temperature (°C)	799,5	663,1	512,6	961,8
Heat rejection to exhaust (kW)	188,662	183,566	175,064	189,728
Power output (kW)	200,079	198,434	195,709	198,762
SFC (g/kWh)	637.2	642.5	651.5	641.5
Thermal efficiency (%)	42.93	42.57	41.99	42.67

Major differences in engine performance under oxyfuel and air combustion are observed in exhaust gas temperature as displayed in Table 9. This was expected due to higher specific heat of carbon dioxide in comparison to that of nitrogen and the much higher concentration compared to water vapor as shown in Fig. 17. At temperatures above 2000 K the heat capacity of the carbon dioxide is almost twice as that of the nitrogen. For the same maximum engine pressure and heat addition, the expected in cylinder peak temperature would be much lower for the oxyfuel combustion products. Even at the onset of ignition, after compression stroke, the reactant mixture will have much lower temperature at oxyfuel combustion mode than that for conventional air combustion, thus reducing the possibility of engine knocking.

Predicted exhaust temperature in oxyfuel combustion varies from 512 to 799 °C, compared to 961 °C for conventional air engine operation. The amount of heat rejected and

engine power output, however, are somehow similar for all the combustion modes being about 183.6 MW for the former and 190 MW for the latter.

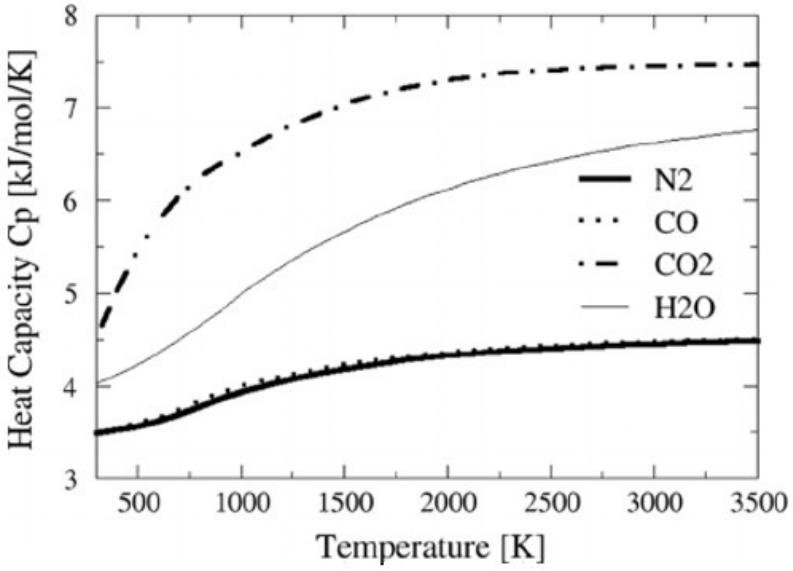

Figure 17 – Heat capacity comparison. [28]

Specific fuel consumptions and engine thermal efficiency are also quite similar for all the cases studied, including the conventional air combustion process.

According to Rayca et al [27], RDF pyrolysis may take place in the temperature range of 400 °C and 900 °C. The exhaust gas temperatures shown in Table 9 varied from about 512 to 799 °C, when operating in the oxyfuel mode. The amount of heat and temperature of flue gases are, therefore, suitable to sustain pyrolysis reactions inside a combined heat and power operation system. For high pyrolysis temperature, 75/25 mixture for oxyfuel combustion would be more appropriate for the CHP plant.

Considering a heat of pyrolysis of about 2,500 kJ/kg, and a 30% gas yields from the thermal degradation of RDF, the reactor claims 295,139 kW of thermal power to sustain the gas production process. The power rejected in exhaust gas amounts 188,662 kW, less than the needed to perform the thermal degradation process. That, however, could be accomplished by burning about 14 ton/h of RDF derived char, with calorific value of 28,000 kJ/kg.

Therefore, the CHP plant is feasible from a technical point of view. In addition, the plant operation under oxyfuel technology would release almost zero emissions of CO_2. Based on these figures we suggest another performance parameter, called total pyro-gas production factor that, for the 72/25 oxyfuel mode, totalizes 639 g/kWh.

Table 10 presents the predicted temperature from the STM model for similar intake conditions (T_1 = 25 °C and P_1 = 1 atm). Thermodynamic state 2 refers to the end of the compression stroke at top dead center and state 3 is that after the heat addition (combustion) in a constant volume process, therefore, at TDC. Thermodynamic state 4 is that at the bottom dead

center, after the compression stroke. At the end of compression stroke, OFC simulation present lower temperatures compared to conventional air combustion. The same behavior was observed during the beginning of heat release. According to Van Blarigan et al [2], higher chamber temperature may cause piston damage and decrease engine longevity, along with knocking tendency. At the end of the combustion process, the temperature for the OFC operation modes varied from 2,700 to 3,036 K, lower than that for CAC, which peaked 3,253 K.

Table 10 – Numerical predictions from the STM model for in OFC and CAC configuration.

In-chamber temperatures	Piston position	CAC	OFC 75/25	OFC 80/20	OFC 85/15
T_2	TDC	791 K	651 K	645 K	637 K
T_3	TDC	3,253 K	3,036 K	2,707 K	2,700 K
T_4	BDC	1,784 K	2,022 K	1,796 K	1,786 K

3.3 FEASIBILITY ANALYSIS

A comprehensive cost analysis should be performed to check the plant's economic feasibility. An expanded overview of powerplant's concept presented in Figure 12 is displayed in Figure 15, along with other supporting facilities.

For cost predictions, oxygen would be provided by a production plant based on cryogenic distillation process, due to its high purity (> 95%) and lower cost when compared to pressure swing adsorption [29].

Some assumptions were made to approach the simulation to an actual intended feasibility analysis. First, it was considered a large-scale state-of-the-art thermoelectric power plant, similar to the Brazilian UTE-LORM, comprised of 24 Wärtsilä 20V34SG gas generator sets with a total combined output of 204 MW [30]. The analysis also refers to an oxyfuel technology implementation on a CHP plant on a 24/7 service.

The payback of the simulated concept is obtained by collecting necessary data from related works and estimates of energy consumption of the associated processes: CPU flue gas compression (MWe); CPU CO2 compression (MWe); Net CPU power consumption (MWe); and ASU power consumption (MWe).

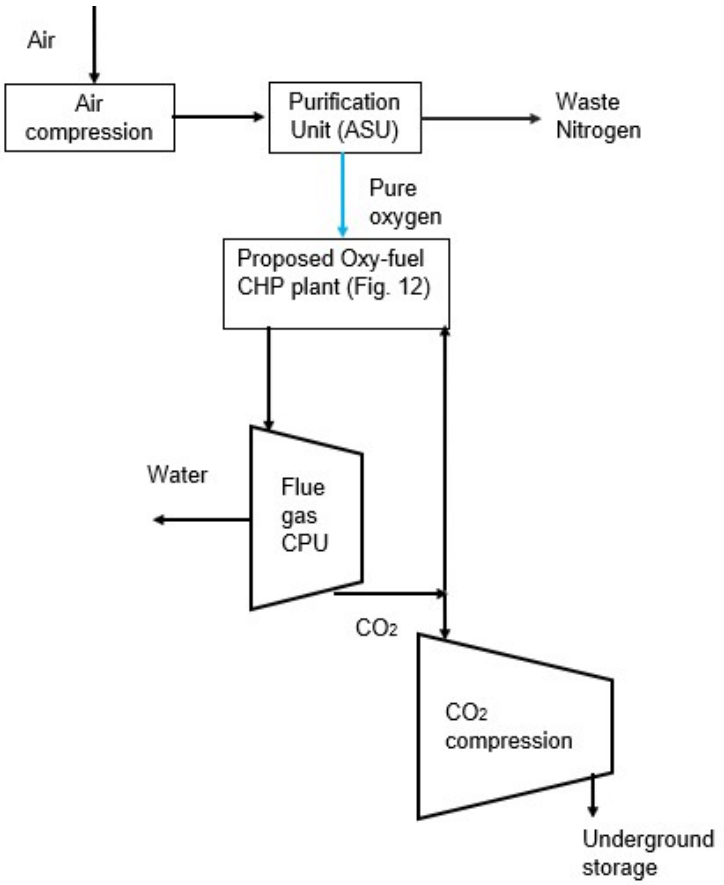

Figure 18 – Expanded facilities containing CCS processes.

The total energy consumption of the operation processes is presented in Eq. (47).

$$I = E + F + G + H \tag{47}$$

Daily total consumption is given by

$$K = IJ \tag{48}$$

Oxygen cost is given by the product of exhaust flow times its production cost

$$O = 0.045N \tag{49}$$

where US$ 0.045/kg corresponds to the price of pure oxygen (>95%) obtained from cryogenic distillation process [29].

Daily facility cost is given by

$$P = KL + 24(M + O) \tag{50}$$

Annual operational costs are obtained by

$$R = 365P \tag{51}$$

Annual cost is the sum of power plant construction cost (US$), Storage plant construction (US$) and daily cost.

$$Q = B + C + 365P \tag{52}$$

Total costs per MWh is

$$S = \frac{P}{K} \tag{53}$$

Daily exhaust mass flow is

$$T = 24(CO_2 \text{ net}) \tag{54}$$

The fixed carbon credit used in this analysis is US$ 36,00 per stored tone. Therefore,

$$U = \text{fixed carbon credit at US\$ } 36{,}00 \tag{55}$$

Carbon credit of exhaust CO_2 is given by

$$V = TU \tag{56}$$

Daily carbon credit income is

$$W = 24V \tag{57}$$

Annual electric energy sales in US$/ year is obtained by

$$AES = 8760LA \tag{58}$$

Annual income ‘X ’is expressed by the combination of carbon credit income and electricity sales, where

$$X = 365W + AES \tag{59}$$

Annual revenue of the proposed facility is the difference between annual carbon income and annual operational costs, given by

$$Y = X - R \tag{60}$$

An average daily revenue could be expressed as

$$Z = \frac{Y}{365} \tag{61}$$

Finally, the payback period is given by

$$\text{Payback} = \frac{B + C}{Y} \tag{62}$$

The following costs were computed:

1) 204 MW power plant construction approximate cost is US$ 102 million, considering 500 US$/kW (Wärtsilä);
2) CCS facility construction cost for natural gas power plant is US$ 172.38 million considering 845 US$/kW, along with ASU's plant cost estimated in US$ 230 million.
3) Pyrolysis plant cost is about US$ 13 million considering US$ 4,700 per kg/h of waste processes and 2,708 kg/h of RDF (30% gas yield);
4) Operational costs [32], [34], [35]:
    a. Flue gas compression and purification unit (CPU) power consumption
    b. CO_2 compression unit power consumption
    c. Air Separation Unit (ASU) power consumption
    d. Fuel cost
    e. Pure oxygen cost
5) Carbon credit [36], [37]

Table 11 summarizes the cost predictions for the proposed CHP plant under CCS technology. The electric power output 200 MW, considering 24 Wärtsilä 20V34SG gas

generator sets operating under oxyfuel combustion using pyrolysis gas from RDF. The CHP-CCS plant would cost less than US$ 512 million, including the gas engines generators, pyrolysis plant, cryogenic air separation unit, and the carbon capture system.

Table 11 – Detailed information of the 75/25 OFC scenario.

Parameter	OFC 75/25
A Power Output (MW)	200
B CHP plant construction cost (US$) + ASU	339.8
C CO2 Capture plant construction (M US$)	172.4
D Operation conditions	-
E CPU flue gas compression (MWe)	14.03
F CPU CO2 compression (MWe)	5.21
G Net CPU power consumption (MWe)	16.9
H ASU power consumption (MWe)	22.57
I Total (MWe)	58.71
J Operating hours	24
K Total per day (MWh)	1,409
L Electricity cost (USD/MWh)	100
M Fuel cost (US$/h)	1,439
N O_2 intake (kg/h)	123,149
O O_2 cost (US$/h)	5541,71
P Daily cost (US$/day)	308,363
Q Cost for 1st year (M US$/year)	624.7
R Annual operational costs (M US$/year)	112,5
S Total costs per MWh (US$/MWh)	218.85
T Capture CO_2 mass flow (CO_2 ton/h)	139.12
U Carbon credit (US$/ton)	36
V Carbon credit of exhaust CO_2 (US$/h)	5.008
W Carbon credit income (US$/day)	120.202
AES Annual Electricity sales (M US$/year)	175,2
X Annual Carbon income (M US$/year)	219,078
Y Annual revenue (M US$/year)	106.4
Z Daily revenue (US$/day)1	291.75
Revenue per MWh (US$/MWh)	207.06
Payback (Years)	4.82

Applying an oxidizer mix of 75% carbon dioxide and 25% of pure oxygen, the total cost of this plant was estimated in 512 million dollars, similar to the other scenarios of OFC technology. Carbon dioxide captured and stored for this 75/25 oxyfuel combustion mode in excess of 3,339 metric tons per day, or about 1.22 million of tons per year. Figure 20 shows the costs associated with installation and operation of the CHP-CCS plant along with the revenue from the power output.

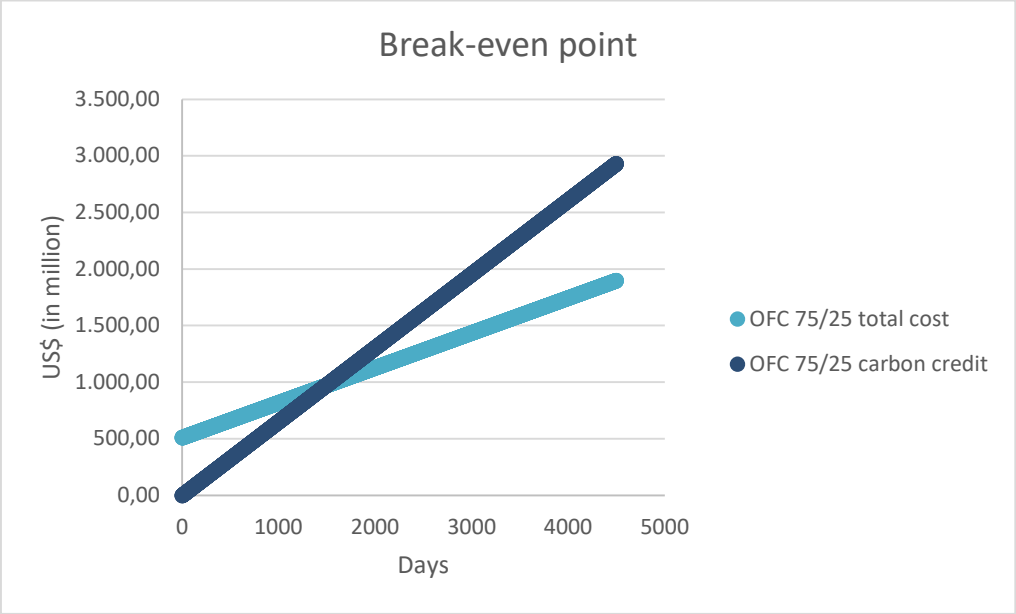

Figure 19 – Break-even point for OFC 75/25.

As it can be seen, the estimated time for the break-even is less than six years, considering the simplified economic analysis. Tozlu et al. [38] performed detailed techno-economic assessment on municipal solid waste-based district heating and electricity production indicating that the CHP plant based on gas turbine would need 4.99 years to break even.

One of the oldest Brazilian waste landfills is located less than 15 miles from the Capital of Brazil (Fig. 20). In 2015 only, it received around 2.8 thousand metric tons of municipal waste and around 6 to 8 thousand tons of construction waste (wood, steel, bricks) daily. [39]

Figure 20 – Brasília's old waste landfill. [40]

The landfill comprised an area of 201 acres and terminated in 2016 as the world's second-largest waste landfill having about 40 (forty) million metric tons [40].

There are serious environmental concerns related to this area; it was transformed into a waste landfill without proper soil sealing, with risks to the water table and soil contamination. It also represents health risks to waste pickers and to the overall population. Since almost 30% of total residues (12 million metric tons) consists of paper and plastic, it could be estimated the time needed to transform and consume this parcel by applying the methodology previously presented in this work. Considering the 204 MW CHP plant, the pyrolysis reactor would process 2.37 million tons of waste per year. Considering an operation period of 10 years, the CHP plant would consume about 24 million tons of RDF, most of the energy fraction from the waste deposited in the Brasilia's landfill.

Chapter 4

4 CONCLUSIONS and FUTURE WORK

Carbon neutrality and waste management are major challenges in the context of increasing population and industrialization, calling for alternative energy sources. In this work, a model was developed to estimate relevant gas engine performance parameters under oxyfuel burning technology for carbon capture and storage of CHP plants. Overall, the mathematical model was considered suitable for the simplified techno-economic analysis.

Numerical predictions showed that oxyfuel combustion of RDF pyrolysis gas in gas engines did not penalize system thermal efficiency. The exhaust gas temperature and heat content are suitable for combined heat and power plants under zero emissions operation.

Despite considering oxyfuel combustion a promising way to reduce and capture carbon dioxide, the technology still faces some obstacles, such as:

- Enormous technology implementation costs due to oxygen production plant and carbon dioxide capture facilities, which may depend on government incentives for project implementation;
- For the simulated 204 MW study, the payback period was of the order of six years, compatible with waste to energy CHP plants (five years), without carbon capture under oxyfuel operation.

  Nevertheless, for future studies an improved economic analysis might be necessary.

5 REFERENCE

[1] BOLOY R, SILVEIRA J, TUNA C, CORONADO C, ANTUNES J. Ecological impacts from syngas burning in internal combustion engine: Technical and Economic aspects. Renewable and Sustainable Energy Reviews. 2011, Vol 15, pp. 5194-5201. DOI: 10.1016/j.rser.2011.04.009

[2] VAN BLARIGAN A, KOZARAC D, SEISER R, CATTOLICA R, CHEN J-Y, DIBBLE R. Experimental Study of Methane Fuel Oxycombustion in a Spark Ignited Engine. Journal of Energy Resources Technology. 2013; 136:012203. https://doi.org/10.1115/1.4024974

[3] SWANTON, C. Scientists discover how air pollution may trigger lung cancer in never-smokers. Sep 10th 2022. Available at https://www.esmo.org/newsroom/press-releases/scientists-discover-how-air-pollution-may-trigger-lung-cancer-in-never-smokers

[4] YANG, Y; LIEW, R; TAMOTHRAN, A.; FOONG, S.; YEK, P.; CHIA, P., VAN TRAN, T.; PENG, W; LAM, S.; Gasification of refuse-derives fuel from municipal solid waste for energy production: a review https://www.ncbi.nlm.nih.gov/pmc/articles/PMC7805569/

[5] YIP, H; SRNA, A; YUEN, A; KOOK, S; TAYLOR, R; YEOH, G; MEDWELL, P; CHAN, Q. A Review of Hydrogen Direct Injection for Internal Combustion Engines: Towards Carbon-Free Combustion. Applied Sciences. 2019, vol 9, 4842, DOI:10.3390/app9224842

[6] WÄRTSILÄ. Combustion Engine vs Gas Turbine: Fuel Flexibility. Accessed April 12th, 2022. https://www.wartsila.com/energy/learn-more/technical-comparisons/combustion-engine-vs-gas-turbine-fuel-flexibility

[7] BOEHMAN A, LE CORRE O. Combustion of Syngas in Internal Combustion Engines. 180:6, 1193-1206, DOI: 10.1080/00102200801963417

[8] COPA J, TUNA C, SILVEIRA J, BOLOY R, BRITO P, SILVA V, CARDOSO J,

EUSÉBIO D. Techno-Economic Assessment of the Use of Syngas Generated from Biomass to Feed an Internal Combustion Engine. Energies 2020, 13, 3097. DOI: 10.3390/en13123097

[9] Siemens Energy. Gas turbines or gas engines? Available at https://www.siemens-energy.com/global/en/offerings/power-generation/rice.html . Last accessed in September 12th 2022.

[10] AZIMOV U.; TOMITA E.; KAWAHARA N.; HARADA Y.; Effect of syngas composition on combustion and exhaust emission characteristics in a pilot-ignited dual-fuel engine operated in PREMIER combustion mode. International Journal of Hydrogen Energy. 2011, Vol. 36, pp. 11985-11996. doi: 10.1016/j.ijhydene.2011.04.192.

[11] XIANG Li, ZHIJUN P, AJMAL T, AITOUCHE A, MOBASHERI R, PEI Y, GAO Bo, WELLERS M. A feasibility study of implementation of oxy-fuel combustion on a practical diesel engine at the economical oxygen-fuel ratios by computer simulation. Advances in Mechanical Engineering 2020, Vol 12(12) 1-13. DOI: 10.1177/1687814020980182.

[12] E. Commission, 2030 climate and energy framework in European Union. Accessed on April 2th 2022. URL: https://ec.europa.eu/clima/policies/strategies/2030_en

[13] Government of Western Australia – Department of Mines, Industry Regulation and Safety – Carbon Capture and Storage. Available at https://www.dmp.wa.gov.au/Petroleum/Carbon-Capture-and-Storage-1599.aspx last accessed in september 6th 2022.

[14] DXP - Pre-combustion vs Post-combustion carbon capture technologies. Available at https://www.dxpe.com/pre-combustion-vs-post-combustion-carbon-capture/ last accessed in September 10th 2022.

[15] J.R. SERRANO, F.J. ARNAU, L.M. GARCÍAC-CUEVAS, V.H. Farias, Oxy-fuel combustion feasibility of compression ignition engines using oxygen separation membranes for enabling carbon dioxide capture, Energy Conversion and Management, Volume 247, 2021, 114732, https://doi.org/10.1016/j.enconman.2021.114732.

[16] MADEJSKI P.; CHMIEL K.; SUBRAMANIAN N.; KUS T. Methods and Techniques for CO_2 Capture: Review of Potential Solutions and Applications in Modern Energy Technologies

Energies 2022, 15, 887. https://doi.org/10.3390/en15030887

[17] PAMMINGER M.; BUYU W.; HALL C.; VOJTECH R.; WALLNER T. The impact of water injection and exhaust gas recirculation on combustion and emissions in a heavy-duty compression ignition engine operated on diesel and gasoline, Int J Engine Res 21 (2019) 146808741881529. DOI:10.1177/1468087418815290.

[18] ZHIHUA W., 1.23 Energy and Air Pollution; Comprehensive Energy Systems, Elsevier, 2018, Pages 909-949, ISBN 9780128149256, https://doi.org/10.1016/B978-0-12-809597-3.00127-9.

[19] SERRANO, J.; MARTÍN, J.; GOMEZ-SORIANO, J.; RAGGI, R. Theoretical and experimental evaluation of the spark-ignition premixed oxy-fuel combustion concept for future CO_2 captive powerplants. Energy conversion and Management, Vol. 244, 2021, 114498, ISSN 0196-8904, https://doi.org/10.1016/j.enconman.2021.114498.

[20] WU, Z-J; YU, X; FU, L-Z; DENG, J; HU, Z-J, LI, L-G. A high efficiency oxyfuel internal combustion engine cycle with water direct injection for waste heat recovery. Energy (2014), http://dx.doi.org/10.1016/j.energy.2014.03.095

[21] SHUDO, T.; NAGANO, T.; KOBAYASHI, M. – Combustion Characteristics of Waste-Pyrolysis Gases in an Internal Combustion Engine. International Journal of Automotive Technology, Vol. 4, N° 1, pp 1-8. 2003.

[22] FIORE, M; MAGI, V; VIGGIANO, A. – Internal combustion engines powered by syngas: A review. Applied energy, Vol. 276, 2020. ISSN 0306-2619 https://doi.org/10.1016/j.apenergy.2020.115415.

[23] MARTIN J, Internal Combustion Engine Course notes, Universidade de Brasília. 2008.

[24] EES,2022. Engineering Equation Solver, F-Chart Software, accessed April 8th, 2022. http://www.fchart.com/ees/

[25] KAMIL M.; RAHMAN M.; BAKAR R.; International Journal of Automotive and Mechanical Engineering (IJAME) ISSN: 2229-8649 (Print); ISSN: 2180-1606 (Online); Volume 9, pp. 1695-1708, June 2014. University Malaysia Pahang.DOI: http://dx.doi.org/10.15282/ijame.9.2013.19.0141

[26] Caterpillar G3520E. Gas Engine Technical Data. Fuel Flexibility. Accessed April 25th 2022. https://emc.cat.com/pubdirect.ashx?media_string_id=GAS-DM8924-02-GS-EPG-M-13100177.pdf

[27] RAYCA P, POSKART A, CHRUBASIK M, SAJDAK M, ZAJEMSKA M, SKIBINSKI A, KOROMBEL A. Technological and economic aspect of Refused Derived Fuel pyrolysis. Renewable Energy, Volume 161, 2020, Pages 482-494, ISSN 0960-1481, https://doi.org/10.1016/j.renene.2020.07.104.

[28] ANDERLOHR, J.; BOUNACEUR, R.; DA CRUZ, A, BATTIN-LECLERC, F. Thermal and Kinetic Impact of CO, CO_2 and H_2O on the Postoxidation of IC-Engine Exhaust Gases. Combustion Science and Technology. 2010. Vol 182. DOI: 10.1080/00102200903190844

[29] ADHIKARI B, ORME C, KLAEHN J, STEWART F. Technoeconomic analysis of oxygen-nitrogen separation for oxygen enrichment using membranes. Separation and Purification Technology 2021. Volume 268, ISSN 1383-5866, https://doi.org/10.1016/j.seppur.2021.118703.

[30] WÄRTSILÄ. Gas and multi-fuel power plants. Accessed May 20th, 2022 https://cdn.wartsila.com/docs/default-source/power-plants-documents/downloads/brochures/gas-and-multi-fuel-power-plants-2017.pdf

[31] U.S. Energy Information Administration – Levelized Costs of New Generation Resources in the Annual Energy Outlook 2022. March 2022.Available At https://www.eia.gov/outlooks/aeo/pdf/electricity_generation.pdf . Last accessed at September 8th 2022.

[32] U.S. Energy Information Administration. Construction cost data for electric generators installed in 2019 – Available at

https://www.eia.gov/electricity/generatorcosts/

[33] Congressional Research Service – Carbon Capture and Sequestration (CCS) in the United States – R44902 – 2021. Available at:
https://sgp.fas.org/crs/misc/R44902.pdf
last accessed in september 9th 2022.

[34] KUJANPÄÄ, L; RITOLA, J; NICKLAS, N; SEBASTIAN, T; Scenarios and new technologies for a North-European CO_2 transport infrastructure in 2050. Energy Procedia. 2014, 63. DOI: 10.1016/j.egypro.2014.11.297
https://www.researchgate.net/figure/Construction-costs-for-the-underground-CO2-storage-facility_tbl1_272380312

[35] KHEIRINIK, M; RAHMANIAN, N. Comparative Techno-Economic Analysis of Carbon Capture Processes: Pre-Combustion, Post-Combustion, and Oxy-Fuel Combustion Operations. Sustainability 2021, 13, 13567. https://doi.org/10.3390/ su132413567

[36] MOCH, J; XUE, W; HOLDREN, J; Carbon capture, utilization and storage: Technologies and Costs in the U.S. Context. Available at: https://www.belfercenter.org/publication/carbon-capture-utilization-and-storage-technologies-and-costs-us-context
last accessed in september 8th 2022.

[37] Congressional Research Service: The Tax Credit for Carbon Sequestration (Section 45Q), 2021, available at: https://sgp.fas.org/crs/misc/IF11455.pdf last accessed in september 8th 2022.

[38] ALPEREN, T; AYSEGUL, A; EMRAH, O; AMJAD, A-M; Municipal solid waste-based district heating and electricity production: A case study. Journal of Cleaner Production,Volume 297, 2021, https://doi.org/10.1016/j.jclepro.2021.126495.

[39] PEREIRA, R.; QUEIROZ, A.; O Lixão de Brasília. Retrato do Brasil. September 2015. Available at: https://observatoriopnrs.files.wordpress.com/2015/10/o-lixc3a3o-de-brasc3adlia-por-rp.pdf . Last accessed in September 10th 2022.

[40] Blog do Riella. Depois de 60 anos, Lixão da Estrutural está sendo desativado. Available at http://blogdoriella.com.br/depois-de-60-anos-lixao-da-estrutural-esta-sendo-desativado/ .Last accessed in September 10th 2022.

[41] Wärtsilä Engines: Wärtsilä 34SG Gas Engine Generation Set. Available at: https://www.wartsila.com/docs/default-source/power-plants-documents/downloads/product-leaflets/w34sg_leaflet.pdf last accessed in september 8th 2022.

APPENDIX I

1.

OFC 75/25

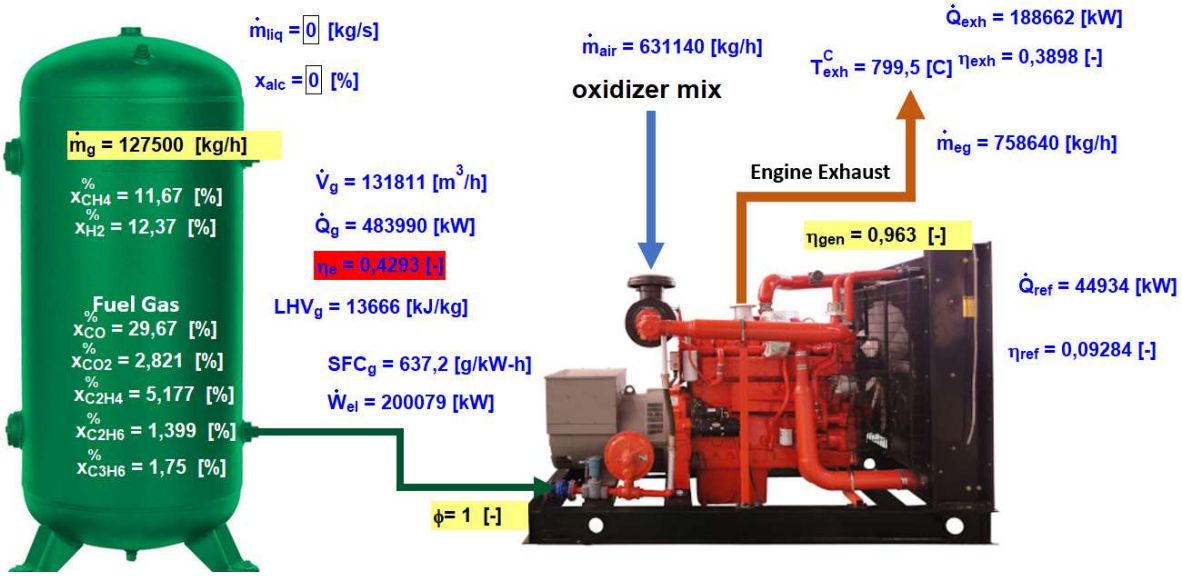

Figure 21 – Interface of Engineering Equation Solver Diagram Window. The green reservoir in the left contains the RDF gas mix. This overview of OFC 75/25 presents most of the relevant data after software calculations, such as electric power, heat rejected and exhaust flow.

OFC 80/20

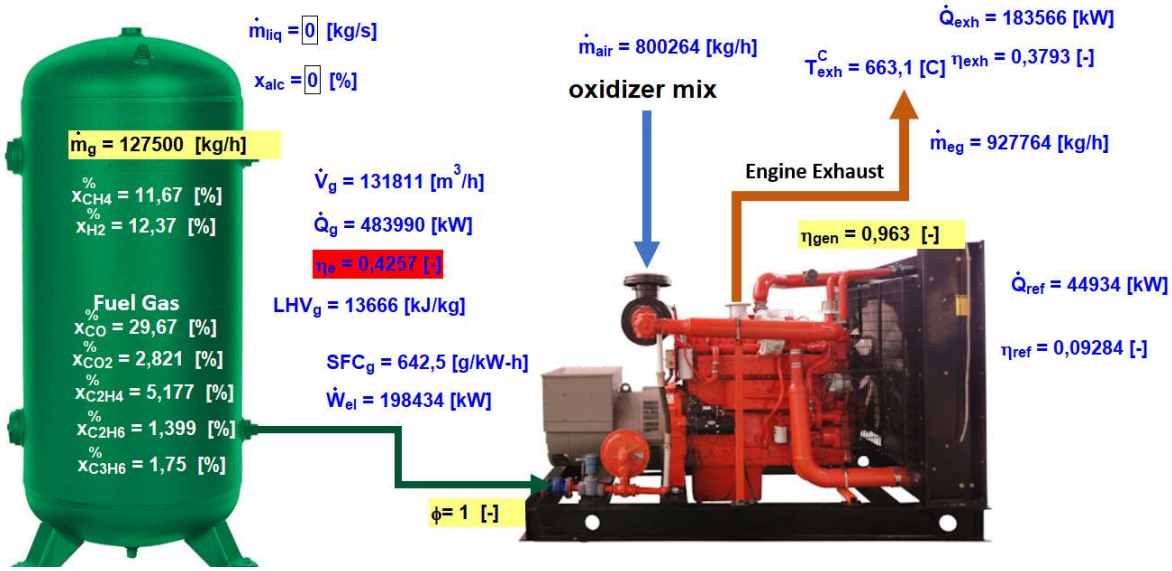

Figure 22 – Interface of Engineering Equation Solver Diagram Window. The green reservoir in the left contains the RDF gas mix. This overview of OFC 80/20 presents most of the relevant data after software calculations, such as electric power, heat rejected and exhaust flow.

OFC 85/15

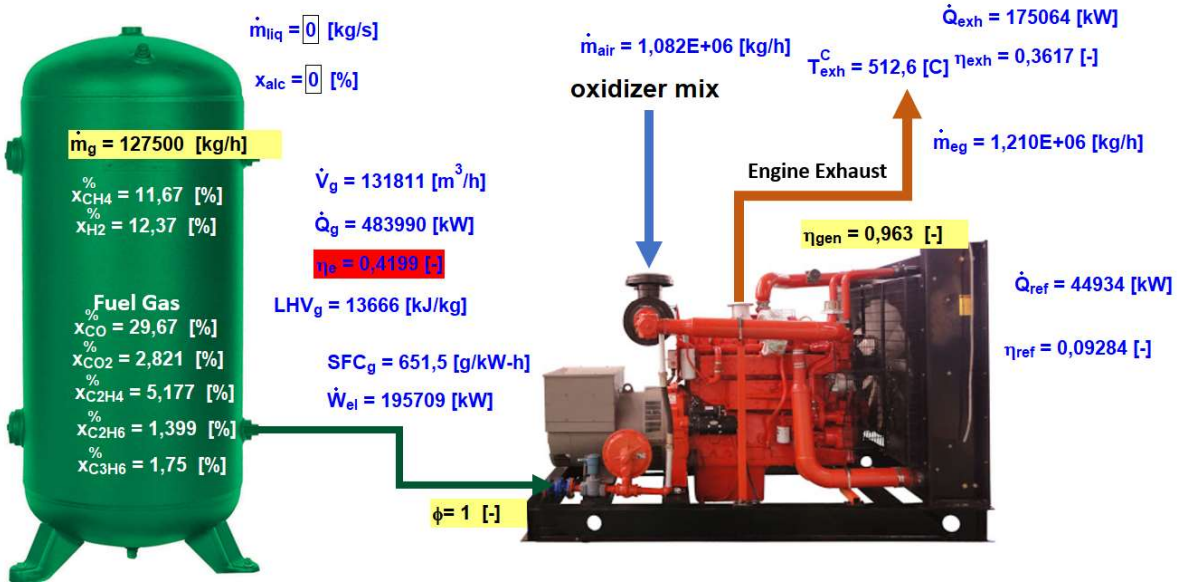

Figure 23 – Interface of Engineering Equation Solver Diagram Window. The green reservoir in the left contains the RDF gas mix. This overview of OFC 85/15 presents most of the relevant data after software calculations, such as electric power, heat rejected and exhaust flow.

2. PAPER PDF;

The authors of this work presented a paper on the 14th International Conference on Applied Energy, held in Bochum, Germany during August 8th -11th 2022. The paper and conference proceedings will be published at Energy Proceedings (ISSN 2004-2965). It has also been selected for the further consideration in Applied Energy and Advances in Applied Energy (ISSN 2666-7924).

G3520E

GAS ENGINE TECHNICAL DATA

CATERPILLAR®

ENGINE SPEED (rpm):	1500	RATING STRATEGY:	HIGH ALTITUDE/AMBIENT
COMPRESSION RATIO:	11.9	PACKAGE TYPE:	WITHOUT RADIATOR
AFTERCOOLER TYPE:	SCAC	RATING LEVEL:	CONTINUOUS
AFTERCOOLER - STAGE 2 INLET (°C):	54	FUEL:	NATURAL GAS
AFTERCOOLER - STAGE 1 INLET (°C):	92	FUEL SYSTEM:	CAT LOW PRESSURE WITH AIR FUEL RATIO CONTROL
JACKET WATER OUTLET (°C):	99		
ASPIRATION:	TA	FUEL PRESSURE RANGE(kPag): (See note 1)	11-35
COOLING SYSTEM:	JW+OC+1AC, 2AC	FUEL METHANE NUMBER:	80
CONTROL SYSTEM:	ADEM3 W/ IM	FUEL LHV (MJ/Nm3):	35.64
EXHAUST MANIFOLD:	DRY	ALTITUDE CAPABILITY AT 25°C INLET AIR TEMP. (m):	2000
COMBUSTION:	LOW EMISSION	POWER FACTOR:	0.8
NOx EMISSION LEVEL (mg/Nm3 NOx):	500	VOLTAGE(V):	400-11000

RATING		NOTES	LOAD	100%	75%	50%
GENSET POWER	(WITHOUT FAN)	2,3	ekW	2022	1517	1015
GENSET POWER	(WITHOUT FAN)	2,3	kVA	2528	1896	1269
ENGINE POWER	(WITHOUT FAN)	3	bkW	2100	1570	1050
GENERATOR EFFICIENCY		2	%	96.3	96.6	96.7
GENSET EFFICIENCY(@ 1.0 Power Factor)	(ISO 3046/1)	4	%	41.5	40.7	38.6
THERMAL EFFICIENCY		5	%	45.3	46.6	49.0
TOTAL EFFICIENCY (@ 1.0 Power Factor)		6	%	86.8	87.3	87.6

ENGINE DATA						
GENSET FUEL CONSUMPTION	(ISO 3046/1)	7	MJ/ekW-hr	8.75	8.93	9.39
GENSET FUEL CONSUMPTION	(NOMINAL)	7	MJ/ekW-hr	8.97	9.15	9.62
ENGINE FUEL CONSUMPTION	(NOMINAL)	7	MJ/bkW-hr	8.63	8.84	9.30
AIR FLOW (0°C, 101.3 kPa)	(WET)	8	Nm3/bkW-hr	3.99	3.96	3.98
AIR FLOW	(WET)	8	kg/bkW-hr	5.16	5.11	5.14
FUEL FLOW (0ºC, 101.3 kPa)			Nm3/hr	509	389	274
COMPRESSOR OUT PRESSURE			kPa(abs)	430	328	235
COMPRESSOR OUT TEMPERATURE			°C	226	184	133
AFTERCOOLER AIR OUT TEMPERATURE			°C	58	58	59
INLET MAN. PRESSURE		9	kPa(abs)	392	294	200
INLET MAN. TEMPERATURE	(MEASURED IN PLENUM)	10	°C	60	60	60
TIMING		11	°BTDC	24	21	16
EXHAUST TEMPERATURE - ENGINE OUTLET		12	°C	430	466	515
EXHAUST GAS FLOW (0 °C, 101.3 kPa)	(WET)	13	Nm3/bkW-hr	4.24	4.21	4.25
EXHAUST GAS MASS FLOW	(WET)	13	kg/bkW-hr	5.34	5.31	5.35
MAX INLET RESTRICTION		14	kPa	2.50	1.96	0.99
MAX EXHAUST RESTRICTION		14	kPa	5.00	2.35	0.22

EMISSIONS DATA - ENGINE OUT						
NOx (as NO2)	(corr. to 5% O2)	15,16	mg/Nm3 DRY	500	500	500
CO	(corr. to 5% O2)	15,17	mg/Nm3 DRY	1153	1081	1096
THC (mol. wt. of 15.84)	(corr. to 5% O2)	15,17	mg/Nm3 DRY	2820	2722	2289
NMHC (mol. wt. of 15.84)	(corr. to 5% O2)	15,17	mg/Nm3 DRY	423	408	343
NMNEHC (VOCs) (mol. wt. of 15.84)	(corr. to 5% O2)	15,17,18	mg/Nm3 DRY	282	272	229
HCHO (Formaldehyde)	(corr. to 5% O2)	15,17	mg/Nm3 DRY	250	247	242
CO2	(corr. to 5% O2)	15,17	g/Nm3 DRY	211	212	211
EXHAUST OXYGEN		15,19	% DRY	9.9	9.6	9.0
LAMBDA		15,19		1.74	1.69	1.61

ENERGY BALANCE DATA						
LHV INPUT		20	kW	5038	3854	2714
HEAT REJECTION TO JACKET WATER (JW)		21,28	kW	655	583	485
HEAT REJECTION TO ATMOSPHERE	(INCLUDES GENERATOR)	22	kW	216	168	127
HEAT REJECTION TO LUBE OIL (OC)		23,28	kW	124	111	94
HEAT REJECTION TO EXHAUST (LHV TO 25°C)		24,25	kW	1462	1166	870
HEAT REJECTION TO EXHAUST (LHV TO 120°C)		24	kW	988	815	643
HEAT REJECTION TO A/C - STAGE 1 (1AC)		26,28	kW	402	205	61
HEAT REJECTION TO A/C - STAGE 2 (2AC)		27,29	kW	157	106	62

CONDITIONS AND DEFINITIONS

Engine rating obtained and presented in accordance with ISO 3046/1. (Standard reference conditions of 25°C, 100 kPa barometric pressure.) No overload permitted at rating shown. Consult the altitude deration factor chart for applications that exceed the rated altitude or temperature.

Emission levels are at engine exhaust flange prior to any after treatment. Values are based on engine operating at steady state conditions, adjusted to the specified NOx level at 100% load and corrected to 5 % exhaust oxygen. Tolerances specified are dependent upon fuel quality. Fuel methane number cannot vary more than ± 3.

For notes information consult page three.

FUEL USAGE GUIDE

CAT METHANE NUMBER	30	35	40	45	50	55	60	65	70	75	80	100
SET POINT TIMING	-	-	-	-	-	16	16	16	16	18	24	24
DERATION FACTOR	0	0	0	0	0	0.75	0.83	0.93	1	1	1	1

ALTITUDE DERATION FACTORS AT RATED SPEED

INLET AIR TEMP °C	0	250	500	750	1000	1250	1500	1750	2000	2250	2500	2750	3000
50	1	1	0.97	0.94	0.91	0.88	0.85	0.82	0.79	0.76	0.73	0.7	0.67
45	1	1	1	1	0.97	0.94	0.91	0.88	0.85	0.82	0.79	0.76	0.73
40	1	1	1	1	1	0.97	0.95	0.92	0.89	0.86	0.84	0.81	0.78
35	1	1	1	1	1	1	1	0.97	0.94	0.91	0.88	0.84	0.81
30	1	1	1	1	1	1	1	1	0.96	0.93	0.89	0.86	0.82
25	1	1	1	1	1	1	1	1	1	0.96	0.92	0.88	0.83
20	1	1	1	1	1	1	1	1	1	0.96	0.92	0.88	0.83
15	1	1	1	1	1	1	1	1	1	0.96	0.92	0.88	0.83
10	1	1	1	1	1	1	1	1	1	0.96	0.92	0.88	0.83

ALTITUDE (METERS ABOVE SEA LEVEL)

AFTERCOOLER HEAT REJECTION FACTORS (ACHRF)

INLET AIR TEMP °C	0	250	500	750	1000	1250	1500	1750	2000	2250	2500	2750	3000
50	1.23	1.26	1.29	1.33	1.36	1.4	1.43	1.47	1.5	1.5	1.5	1.5	1.5
45	1.18	1.21	1.24	1.28	1.31	1.34	1.38	1.41	1.45	1.45	1.45	1.45	1.45
40	1.13	1.16	1.19	1.23	1.26	1.29	1.33	1.36	1.4	1.4	1.4	1.4	1.4
35	1.08	1.11	1.14	1.17	1.21	1.24	1.27	1.31	1.34	1.34	1.34	1.34	1.34
30	1.03	1.06	1.09	1.12	1.16	1.19	1.22	1.26	1.29	1.29	1.29	1.29	1.29
25	1	1.01	1.04	1.07	1.1	1.14	1.17	1.2	1.24	1.24	1.24	1.24	1.24
20	1	1	1	1.02	1.05	1.08	1.12	1.15	1.18	1.18	1.18	1.18	1.18
15	1	1	1	1	1	1.03	1.06	1.1	1.13	1.13	1.13	1.13	1.13
10	1	1	1	1	1	1	1.01	1.04	1.07	1.07	1.07	1.07	1.07

ALTITUDE (METERS ABOVE SEA LEVEL)

FUEL USAGE GUIDE:
This table shows the derate factor and full load set point timing required for a given fuel. Note that deration and set point timing adjustment may be required as the methane number decreases. Methane number is a scale to measure detonation characteristics of various fuels. The methane number of a fuel is determined by using the Caterpillar methane number calculation.

ALTITUDE DERATION FACTORS:
This table shows the deration required for various air inlet temperatures and altitudes. Use this information along with the fuel usage guide chart to help determine actual engine power for your site. The derate factors shown do not account for the external cooling system capacity. The derate factors provided assume the external cooling system can maintain the specified cooling water temperatures at site conditions.

ACTUAL ENGINE RATING:
To determine the actual rating of the engine at site conditions, one must consider separately, limitations due to fuel characteristics and air system limitations. The Fuel Usage Guide deration establishes fuel limitations. The Altitude/Temperature deration factors and RPC (reference the Caterpillar Methane Program) establish air system limitations. RPC comes into play when the Altitude/Temperature deration is less than 1.0 (100%). Under this condition, add the two factors together. When the site conditions do not require an Altitude/Temperature derate (factor is 1.0), it is assumed the turbocharger has sufficient capability to overcome the low fuel relative power, and RPC is ignored. To determine the actual power available, take the lowest rating between 1) and 2).
1) Fuel Usage Guide Deration
2) 1-((1-Altitude/Temperature Deration) + (1-RPC))

AFTERCOOLER HEAT REJECTION FACTORS(ACHRF):
To maintain a constant air inlet manifold temperature, as the inlet air temperature goes up, so must the heat rejection. As altitude increases, the turbocharger must work harder to overcome the lower atmospheric pressure. This increases the amount of heat that must be removed from the inlet air by the aftercooler. Use the aftercooler heat rejection factor (ACHRF) to adjust for inlet air temp and altitude conditions. See notes 28 and 29 for application of this factor in calculating the heat exchanger sizing criteria. Failure to properly account for these factors could result in detonation and cause the engine to shutdown or fail.

INLET AND EXHAUST RESTRICTIONS FOR ALTITUDE CAPABILITY:
The altitude derate chart is based on the maximum inlet and exhaust restrictions provided on page 1. Contact factory for restrictions over the specified values. Heavy Derates for higher restrictions will apply.

NOTES:
1. Fuel pressure range specified is to the engine fuel control valve. Additional fuel train components should be considered in pressure and flow calculations.
2. Generator efficiencies, power factor, and voltage are based on standard generator. [Genset Power (ekW) is calculated as: Engine Power (bkW) x Generator Efficiency], [Genset Power (kVA) is calculated as: Engine Power (bkW) x Generator Efficiency / Power Factor]
3. Rating is without engine driven water pumps. Tolerance is (+)3, (-)0% of full load.
4. Genset Efficiency published in accordance with ISO 3046/1, based on a 1.0 power factor.
5. Thermal Efficiency is calculated based on energy recovery from the jacket water, lube oil, 1st stage aftercooler, and exhaust to 120ºC with engine operation at ISO 3046/1 Genset Efficiency, and assumes unburned fuel is converted in an oxidation catalyst.
6. Total efficiency is calculated as: Genset Efficiency + Thermal Efficiency. Tolerance is ±10% of full load data.
7. ISO 3046/1 Genset fuel consumption tolerance is (+)5, (-)0% at the specified power factor. Nominal genset and engine fuel consumption tolerance is ± 2.5% of full load data at the specified power factor.
8. Air flow value is on a 'wet' basis. Flow is a nominal value with a tolerance of ± 5 %.
9. Inlet manifold pressure is a nominal value with a tolerance of ± 5 %.
10. Inlet manifold temperature is a nominal value with a tolerance of ± 5°C.
11. Timing indicated is for use with the minimum fuel methane number specified. Consult the appropriate fuel usage guide for timing at other methane numbers.
12. Exhaust temperature is a nominal value with a tolerance of (+)35°C, (-)30°C.
13. Exhaust flow value is on a 'wet' basis. Flow is a nominal value with a tolerance of ± 6 %.
14. Inlet and Exhaust Restrictions are maximum allowed values at the corresponding loads. Increasing restrictions beyond what is specified will result in a significant engine derate.
15. Emissions data is at engine exhaust flange prior to any after treatment.
16. NOx tolerances are ± 18% of specified value.
17. CO, CO2, THC, NMHC, NMNEHC, and HCHO values are "Not to Exceed" levels. THC, NMHC, and NMNEHC do not include aldehydes.
18. VOCs - Volatile organic compounds as defined in US EPA 40 CFR 60, subpart JJJJ
19. Exhaust Oxygen tolerance is ± 0.5; Lambda tolerance is ± 0.05. Lambda and Exhaust Oxygen level are the result of adjusting the engine to operate at the specified NOx level.
20. LHV rate tolerance is ± 2.5%.
21. Heat rejection to jacket water value displayed includes heat to jacket water alone. Value is based on treated water. Tolerance is ± 10% of full load data.
22. Heat rejection to atmosphere based on treated water. Tolerance is ± 50% of full load data.
23. Lube oil heat rate based on treated water. Tolerance is ± 20% of full load data.
24. Exhaust heat rate based on treated water. Tolerance is ± 10% of full load data.
25. Heat rejection to exhaust (LHV to 25°C) value shown includes unburned fuel and is not intended to be used for sizing or recovery calculations.
26. Heat rejection to A/C - Stage 1 based on treated water. Tolerance is ±5% of full load data.
27. Heat rejection to A/C - Stage 2 based on treated water. Tolerance is ±5% of full load data.
28. Total Jacket Water Circuit heat rejection is calculated as: (JW x 1.1) + (OC x 1.2) + (1AC x 1.05) + [0.9 x (1AC + 2AC) x (ACHRF - 1) x 1.05]. Heat exchanger sizing criterion is maximum circuit heat rejection at site conditions, with applied tolerances. A cooling system safety factor may be multiplied by the total circuit heat rejection to provide additional margin.
29. Total Second Stage Aftercooler Circuit heat rejection is calculated as: (2AC x 1.05) + [(1AC + 2AC) x 0.1 x (ACHRF - 1) x 1.05]. Heat exchanger sizing criterion is maximum circuit heat rejection at site conditions, with applied tolerances. A cooling system safety factor may be multiplied by the total circuit heat rejection to provide additional margin.

FREE FIELD MECHANICAL & EXHAUST NOISE

MECHANICAL: Sound Power (1/3 Octave Frequencies)

Gen Power Without Fan	Percent Load	Engine Power	Overall	100 Hz	125 Hz	160 Hz	200 Hz	250 Hz	315 Hz	400 Hz	500 Hz	630 Hz	800 Hz
ekW	%	bkW	dB(A)	dB(A)	dB(A)	dB(A)	dB(A)	dB(A)	dB(A)	dB(A)	dB(A)	dB(A)	dB(A)
2022	100	2100	119.3	79.4	96.3	96.7	94.3	96.9	101.5	103.7	102.6	103.5	105.3
1517	75	1570	118.2	77.0	92.8	95.0	91.9	95.0	97.8	99.6	101.1	101.3	102.2
1015	50	1050	114.0	75.3	88.9	89.4	88.1	90.4	94.0	95.0	100.1	100.3	100.3

MECHANICAL: Sound Power (1/3 Octave Frequencies)

Gen Power Without Fan	Percent Load	Engine Power	1 kHz	1.25 kHz	1.6 kHz	2 kHz	2.5 kHz	3.15 kHz	4 kHz	5 kHz	6.3 kHz	8 kHz	10 kHz
ekW	%	bkW	dB(A)	dB(A)	dB(A)	dB(A)	dB(A)	dB(A)	dB(A)	dB(A)	dB(A)	dB(A)	dB(A)
2022	100	2100	106.6	107.5	108.0	106.6	107.2	107.5	103.6	109.7	114.2	103.6	98.2
1517	75	1570	104.5	104.1	105.4	104.1	103.5	104.0	104.0	115.7	101.9	100.7	99.4
1015	50	1050	103.3	101.2	102.4	101.8	102.2	102.5	107.6	101.3	98.2	104.4	93.3

EXHAUST: Sound Power (1/3 Octave Frequencies)

Gen Power Without Fan	Percent Load	Engine Power	Overall	100 Hz	125 Hz	160 Hz	200 Hz	250 Hz	315 Hz	400 Hz	500 Hz	630 Hz	800 Hz
ekW	%	bkW	dB(A)	dB(A)	dB(A)	dB(A)	dB(A)	dB(A)	dB(A)	dB(A)	dB(A)	dB(A)	dB(A)
2022	100	2100	124.9	95.1	103.9	108.9	113.5	113.0	110.2	112.4	111.9	113.2	112.8
1517	75	1570	121.8	91.9	103.7	109.3	111.7	105.6	100.4	101.5	103.5	103.2	101.6
1015	50	1050	118.7	92.4	102.2	106.6	109.3	104.4	95.8	97.3	98.9	99.6	100.1

EXHAUST: Sound Power (1/3 Octave Frequencies)

Gen Power Without Fan	Percent Load	Engine Power	1 kHz	1.25 kHz	1.6 kHz	2 kHz	2.5 kHz	3.15 kHz	4 kHz	5 kHz	6.3 kHz	8 kHz	10 kHz
ekW	%	bkW	dB(A)	dB(A)	dB(A)	dB(A)	dB(A)	dB(A)	dB(A)	dB(A)	dB(A)	dB(A)	dB(A)
2022	100	2100	112.4	112.6	112.9	112.0	112.5	112.8	113.3	111.6	112.8	110.0	105.0
1517	75	1570	103.4	104.5	107.5	108.0	111.0	114.1	111.9	114.2	110.4	106.3	104.5
1015	50	1050	102.2	102.1	105.8	108.1	109.6	109.2	109.6	107.6	105.4	104.6	99.2

SOUND PARAMETER DEFINITION:
Sound Power Level Data - DM8702-03

Sound power is defined as the total sound energy emanating from a source irrespective of direction or distance. Sound power level data is presented under two index headings:
Sound power level -- Mechanical
Sound power level -- Exhaust

Mechanical: Sound power level data is calculated in accordance with ISO 3747. The data is recorded with the exhaust sound source isolated.

Exhaust: Sound power level data is calculated in accordance with ISO 6798 Annex A. Exhaust data is post-catalyst on gas engine ratings labeled as "Integrated Catalyst".

Measurements made in accordance with ISO 3747 and ISO 6798 for mechanical and exhaust sound level only. Frequency bands outside the displayed ranges are not measured, due to physical test, and environmental conditions that affect the accuracy of the measurement. No cooling system noise is included unless specifically indicated. Sound level data is indicative of noise levels recorded on one engine sample in a survey grade 3 environment.

How an engine is packaged, installed and the site acoustical environment will affect the site specific sound levels. For site specific sound level guarantees, sound data collection needs to be done on-site or under similar conditions.

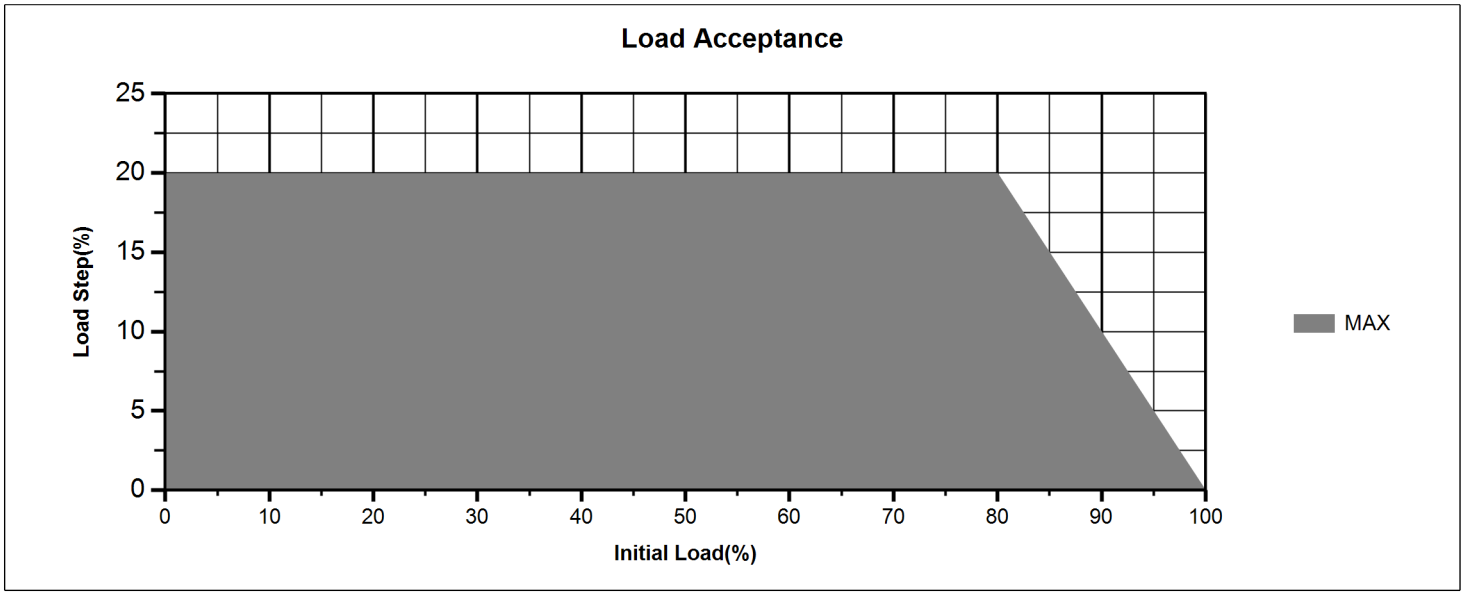

Transient Load Acceptance

Load Step	Frequency Deviation +/- (%)	Voltage Deviation +/- (%)	Recovery Time (sec)	Classification as Defined by ISO 8528 - 5	Notes
20	+20/-20	+20/-20	30		
15	+20/-16	+15/-15	25		
10	+14/-14	+10/-10	15		
5	+8/-8	+6/-6	14		
-5	+8/-8	+6/-6	14		
-10	+14/-14	+10/-10	15		
-15	+20/-16	+15/-15	25		
Breaker Open	+25/-25	+35/-35	40		(1)
Recovery Specification	+1.75/-1.75	+5/-5			
Steady State Specification	+1/-1	+5/-5			(2)

Transient Information

The transient load steps listed above are stated as a percentage of the engine's full rated load as indicated in the appropriate performance technical data sheet. Site ambient conditions, fuel quality, inlet/exhaust restriction and emissions settings will all affect engine response to load change. Engines that are not operating at the standard conditions stated in the Technical data sheet should be set up according to the guidelines included in the technical data; applying timing changes and/or engine derates as needed. Adherence to the engine settings guidelines will allow the engines to retain the transient performance stated in the tables above as a percentage of the site derated power (where appropriate).Fuel supply pressure and stability is critical to transient performance. Proper installation requires that all fuel train components (including filters, shut off valves, and regulators) be sized to ensure adequate fuel be delivered to the engine. The following are fuel pressure requirements to be measured at the engine mounted fuel control valve.

a. Steady State Fuel Pressure Stability +/- 1 kPa/sec
b. Transient fuel Pressure Stability +/- 1 kPa/sec

Inlet water temperature to the SCAC must be maintained at specified value for all engines. It is important that the external cooling system design is able to maintain the Inlet water temp to the SCAC to within +/- 1 °C during all engine-operating cycles. The SCAC inlet temperature stability criterion is to maintain stable inlet manifold air temperature. The Air Fuel Ratio control system requires up to 180 seconds to converge after a load step has been performed for NOx to return to nominal setting. If the stabilization time is not met between load steps the transient performance listed in the document may not be met. Differences in generator inertia may change the transient response of engine. Engine Governor gains and Voltage regulator settings may need to be tuned for site conditions. The time needed to start and stabilize at rated engine speed is a minimum of 60 seconds after a successful crank cycle. Engines must be maintained in accordance to guidelines specified in the Caterpillar Service Manuals applicable to each engine. Wear of components outside of the specified tolerances will affect the transient capability of the engine.Transient performance data is representative of a "Hot" (previously loaded or fully heat soaked) genset.

NOTES:

1. For unloading the engine to 0% load from a loaded condition an external input has been provided. The intention of the Breaker Switch is to be connected to the local generator breaker. In the event that the local generator breaker opens the breaker switch provides an input to the engine controller that resets all control inputs to the rated idle condition. This prevents engine over speeding and will allow the engine to remain running unloaded at the rated synchronous speed. The breaker switch cannot be used to transition down from one loaded state to another. Only when transitioning from a loaded state to 0% load. The breaker switch must change states with 0.2 seconds of the breaker opening otherwise engine over speed or backfire may occur.
2. Steady state voltage and frequency stability specified at +/-2 sigma or better.

Certificate of Participation

This is to certify that

Andrew Cantanhede Cardoso

has participated in the International Conference of Applied Energy 2022 during Aug 8-11, 2022, Bochum, Germany & Virtual

Paper ID: 528

Paper title: Gas engine Oxy Fuel Combustion for Combined Heat and Power Applications

Prof. J. Yan
Conference Chair of ICAE 2022
& Editor-in-Chief of *Advances in Applied Energy*

Energy Proceedings
2022
ISSN 2004-2965

Gas engine Oxy Fuel Combustion for Combined Heat and Power Applications

Andrew Cantanhede Cardoso[1], Carlos Alberto Gurgel Veras[2]

1 University of Brasília – Graduate Program in Mechanical Sciences

2 University of Brasília – Energy and Environment Laboratory – University of Brasília – LEA-UnB

ABSTRACT

Oxy-fuel combustion (OFC) is a promising technology for Carbon Capturing and Storage (CCS) in power generation systems. This work presents a mathematical model to predict relevant gas engine parameters for combined heat and power application. Different oxidizer blends (O2 + CO2) for the combustion of refuse-derived fuel pyrolysis gas were tested. Numerical predictions showed that oxy-fuel combustion of RDF pyrolysis gas in power engines did not penalize system thermal efficiency. The exhaust gas temperature and heat content suit combined heat and power plants under zero emissions operation.

Keywords: gas engine, carbon capture and storage, oxy-fuel combustion, waste management, pyrolysis, combined heat and power.

NOMENCLATURE

Abbreviations	
CAC	Conventional Air Combustion
CCS	Carbon Capture and Storage
EGR	Exhaust Gas Recirculation
ICE	Internal Combustion Engine
ICEG	Internal Combustion Engine-Generator
LHV	Lower Heating Value
OFC	Oxy-Fuel Combustion
RDF	Refused-Derived Fuel
SFC	Specific Fuel Consumption
WtE	Waste to Energy
Symbols	
AFR_{mb}	Stoichiometric ratio mass based
AFR_{vb}	Stoichiometric ratio volume based
c_p	Average specific heat capacity of the mix, constant pressure
c_v	Average specific heat capacity of the mix, constant volume
D	Piston bore
h_{in}	Enthalpy of reactants
h_{out}	Enthalpy of products
k_s	Dry friction loss factor
k_w	Wet friction loss factor
$\dot{m}_{oxid}$	Oxidizer mass flow
$\dot{m}_{in}$	Mass input flow
$\dot{m}_{out}$	Mass output flow
$\dot{m}_{eg}$	Exhaust gas flow
N	Cycle strokes
P_e	Engine power
$\bar{p}_c$	Mean compression pressure
$\bar{p}_e$	Mean effective pressure
$\bar{p}_f$	Mean friction pressure
$\bar{p}_{f,0}$	Constant dry friction pressure
$\bar{p}_i$	Mean indicated pressure
r	Charging coefficient
R	Universal gas constant
rpm	Engine speed (cycle per minute)
V_c	Engine total displacement
w	Piston mean velocity
Greek Symbols	
β	Number of CO_2 moles in the oxidizer mix
Δp_r	Pressure difference between exhaust and intake
γ	Number of N_2 moles in the oxidizer mix
$\gamma(T)$	Specific heat ratio
ξ	Convenience factor
ε_E	Engine coefficient losses for exhaust gases
ε_P	Engine coefficient losses for heat transfer to walls (cooling)
ε_R	Engine coefficient losses for air intake
ϕ	Fuel air equivalence ratio
η_e	Engine effective efficiency
η_i	Engine internal efficiency
η_{ind}	Engine indicated efficiency
η_{isc}	Compressor isentropic efficiency
η_{isT}	Turbine isentropic efficiency
η_{mec}	Engine mechanical efficiency
η_{th}	Engine thermal efficiency
ρ_0	Reactants mix density
χ	Compression ratio

This is a paper for the 14th International Conference on Applied Energy - ICAE2022, Aug. 8-11, 2022, Bochum, Germany.

1. INTRODUCTION

Reduction of greenhouse gas emissions claims alternative power generation fuels [1] and advanced burning technologies [2] also avoiding gases that lead to air quality deterioration such as NO_x, carbon monoxide (CO) and hydrocarbons (HC) [3]. The European Union, for instance, has defined ambitious targets for 2030, cutting no less than 40% in greenhouse gas emissions (CO_2, CH_4, N_2O, etc.) from 1990 levels, and improving about 32% overall energy transformation efficiency [4]. Carbon Capture and Storage (CCS) technology combined with more efficient power generation would further reduce CO_2 emissions [5]. Renewable energy sources also play a major role to substitute fossil fuels in any combined strategy to decrease greenhouse gas emissions.

In terms of power generation, Internal Combustion Engines-Generators (ICEGs) play a significant role in developing countries [6] due to their lower cost, larger availability and better fuel flexibility [7] when compared to gas turbines [8]. In Brazil, gas engines have been the preferred technology for landfill gas utilization in WtE projects.

There are few works, however, dealing with oxy-fuel technology in ICE's. This work thus investigates the use of pyrolysis gas from Refuse-Derived Fuels in internal combustion engines running in oxy-fuel mode. Engine operation was modeled to provide relevant data for combined heat and power assessment under oxy-fuel combustion.

2. OXY-FUEL COMBUSTION IN ICE'S

Oxy-fuel combustion relies on using oxygen diluted in recycled carbon dioxide [9] whose combustion process is given by

$$C_xH_yO_z + a(O_2 + \alpha CO_2) \rightarrow bCO_2 + cH_2O \qquad \text{Equation 1.}$$

The CO_2 stoichiometric coefficient (α) may be adjusted for improved system efficiency based on the adopted heat conversion technology. The flue gas is then cooled to condense the water vapor and the captured excess carbon dioxide is stored underground.

According to Rajca et al. [10], gas obtained from RDF pyrolysis has a calorific value in the range of 15-30 MJ/Nm³. The pyrolysis gas is a mixture of varying concentrations of CO, CO_2, CH_4, H_2 and other minor constituents. The fuel is therefore appropriated for OFC technology in terms of energy density and composition.

To perform this goal, a set of equations proposed by Martin [11] were programmed in the Engineering Equation Solver platform [12]. The combined heat and power system is depicted in Fig. 1. Basically, an ICE burns RDF pyrolysis gas under oxy-fuel mode. Oxygen would be provided by a production plant based on cryogenic distillation process, due to its high purity (>95%) and lower cost when compared to pressure swing adsorption [13].

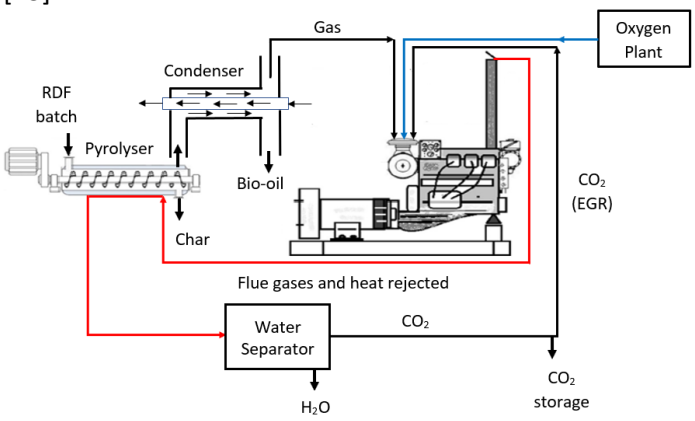

Fig. 1 – CHP plant for oxy-fuel application.

3. METHODOLOGY

3.1 Combustion Engine Modelling

The theory lies on solving a set of thermodynamic equations of a standard four-stroke Otto cycle. The cycle is comprised of an adiabatic irreversible compression (stage 1 to 2), energy addition at near constant volume (stage 2 to 3) irreversible expansion (state 3 to 4), and idealized heat rejection, also at constant volume, to close the cycle (stage 4 to 1). The ideal gas law is used to determine the thermodynamic states.

The model is based on the main processes that take place along the cycle [11]:

$$\eta_{ind} + \varepsilon_P + \varepsilon_E + \varepsilon_R = 1 \qquad \text{Equation 2}$$

In Equation 2, the main processes are given by the indicated engine efficiency from the heat addition (η_{ind}), cooling losses through cylinder walls (ε_P), losses from the exhaust (ε_E), and intake breathing losses (ε_R). Cooling losses depend on the charging coefficient (r), mean piston velocity (w), diameter (D), and the compression ratio (χ):

$$\varepsilon_P = 0.015 \cdot (r \cdot w \cdot D)^{-0,2} \cdot (\chi^{0,8} + 3\,\chi^{-0,4}) \qquad \text{Equation 3}$$

where the charging coefficient is given by

$$r = \left(\eta_{isc}\eta_{isT}\frac{\dot{m}_{eg}h_{inT}}{\dot{m}_{oxid}h_{in_{oxid}}}\right)^{\frac{\gamma(T)}{\gamma(T)-1}}\frac{T_{in_{oxid}}}{T_{out_{oxid}}} \qquad \text{Equation 4}$$

Mixture specific heat capacities, at both constant pressure and constant volume, at any given temperature are calculated with the following equation

$$\gamma(T) = \sum \frac{Y_i c_{p_i}(T)}{Y_i c_{v_i}(T)} \qquad \text{Equation 5}$$

For gaseous fuels, intake breathing losses ε_R are inferred by

$$\varepsilon_R = \frac{\Delta p_R}{r \cdot \rho_0 \cdot \left(\frac{AFR_{vb}}{AFR_{vb}+\phi}\right) \cdot \phi \cdot \frac{LHV}{AFR_{mb}}} \qquad \text{Equation 6}$$

where Δp_R is the difference between exhaust (p_{exh}) and intake (p_{int}) pressures.
Losses from the exhaust are calculated by

$$\varepsilon_E = \frac{1}{\chi^{\xi}} - \varepsilon_P \left(\frac{2}{\chi^{\xi}+1}\right) \qquad \text{Equation 7}$$

where the convenience factor ξ is obtained for the thermodynamic cycle with varying properties, $\gamma = f(T)$,

$$\xi = 0.277 + 0.06(1 - \phi + (1 - 0.1\chi^{0.5})(1 - \phi)^{2,5}) \qquad \text{Equation 8}$$

The overall engine performance can be inferred through a set of equations that are a function of engine sizing, operation regime, fuel type, mechanical friction and mixture compression losses. The losses are established by a set of mean engine pressures. The indicated efficiency in Equation 2 is calculated from the mechanical and effective efficiencies:

$$\eta_e = \eta_{mec}\eta_{ind} \qquad \text{Equation 9}$$

where

$$\eta_{mec} = 1 - \frac{\bar{p}_f}{\bar{p}_i} \qquad \text{Equation 10}$$

In equation 10, average piston friction pressure due to piston rings and lubrication is given by

$$\bar{p}_f = \bar{p}_{f,0} + k_s(2\bar{p}_c + \bar{p}_i)k_w \frac{w}{D} \qquad \text{Equation 11}$$

and mean indicated pressure is inferred with

$$\bar{p}_i = \eta_{ind} r \rho_0 \frac{AFR_{vb}}{(AFR_{vb}+\phi)} \frac{\phi LHV}{AFR_{mb}} \qquad \text{Equation 12}$$

The effective efficiency is calculated from the engine brake power which is a function of the mean effective pressure, engine total displacement, speed, and cycle regime:

$$P_e = \bar{p}_e V_c \frac{rpm}{N} \qquad \text{Equation 13}$$

where

$$\bar{p}_e = \eta_e r \rho_0 \frac{AFR_{vb}}{(AFR_{vb}+\phi)} \frac{\phi LHV}{AFR_{mb}} \qquad \text{Equation 14}$$

The fundamental equations from 2 to 14 were implemented in the EES platform, along with a set of auxiliary equations in order to get relevant engine performance data for combined heat and power applications under CCS technology. A total of 137 equations comprised the model for the oxy-fuel CHP plant.

The presented model was first validated by comparing numerical predictions with performance data of a commercial gas engine (Caterpillar G3520) [14].

For that, it was assumed: $\bar{p}_{f,0} = 70\ kPa$, $k_s = 0{,}02\ kPa$, $k_w = 0{,}70\ kPa$, $\bar{p}_c = 700\ kPa$ for electric generators powered by a gas engine [11].

Validation results and corresponding catalog reference information are presented in Table 1. Similar results were obtained for natural gas and ϕ = 0,57 from the manufacturer's datasheet. As it can be seen, the model is capable of reproducing with a high level of confidence the basic operation of an actual engine. Therefore, relevant data can be obtained for combined heat and power systems assessment.

Table 1 – Code validation.

Parameter	CAC ϕ=0.57	G3520 ϕ=0.57
Thermal efficiency (%)	42.4	45.3
Exhaust gas temperature (°C)	496.4	430
SFC (MJ/kWh)	8.81	8.63
Exhaust heat rejection (kW)	1682	1462
Power output (kW)	2085	2100

4. RESULTS AND DISCUSSION

The model was then applied to simulate different oxidizer compositions (OFC) as presented in table 2 burning RDF pyrolysis. Refuse-Derived Fuel (RDF) pyrolysis gas composition is presented in Table 3 [10].

Table 2 - Oxidizer mixes - Species vol (%)

OFC		CAC	
CO_2	O_2	N_2	O_2
75/80/85	25/20/15	78	21

For fuel and oxidizer compositions used in OFC and CFC simulations, major differences in engine performance are related to the exhaust gas temperature. This was expected due to the larger specific heat of carbon dioxide in comparison to that of nitrogen and the much higher concentration compared to that of water vapor, which has higher specific heat. Exhaust gas temperature and heat rejection for the OFC varies by less than 38% and 8%, respectively. Every 5% increase in CO_2 oxidizer concentration implies a minimum 150 °C drop in exhaust gas temperature while generating an increment

in carbon capture by at least 25% as compared to conventional air combustion.

Table 3 - Fuel composition (RDF) – main species concentration (%)

C_2H_6	C_3H_6	CO_2	H_2	C_2H_4	CH_4	CO
4.3	7.1	11.8	12.4	13.8	17.8	29.6

Table 4 – Numerical predictions for OFC and CAC burning modes.

	OFC 75/25 (ϕ=1)	OFC 80/20 (ϕ=1)	OFC 85/15 (ϕ=1)	CAC (ϕ=1)
CO_2 (exhaust %)	87.2	89.3	91.9	13.5
H_2O (exhaust %)	12.4	9.8	7.4	15.8
N_2 (exhaust %)	0.4	0.9	0.7	70.7
Exhaust mass flow (kg/h)	7542	9430	12578	6529
Exhaust temperature (°C)	846	694.3	530.8	965.3
Heat rejection to exhaust (kW)	2097	2040	1945	2128
Power output (kW)	2217	2200	2172	2223
SFC (MJ/kWh)	8.694	8.76	8.873	8.747
Thermal efficiency (%)	43.01	42.67	42.13	42.74

For the same power input and engine operational conditions, slightly different exhaust gas concentrations of H_2O and CO_2 were obtained by varying the oxidizer composition in OFC mode, as presented in Table 4. Specific fuel consumptions and engine thermal efficiency are also quite similar for all the cases studied, including the conventional combustion process.

According to Rayca et al [10], RDF pyrolysis may take place in the temperature range of 400 °C and 900 °C. The exhaust gas temperatures shown in Table 4 varied from about 530 to 846 °C, when operating in the oxyfuel mode. The amount of heat and the temperature of the flue gases are, therefore, suitable to sustain the pyrolysis reactions inside in combined heat and power operation system. Considering a heat of pyrolysis of about 2500 kJ/kg, the heat rejected by the engine would process near 3000 kg/h of RDF. The CHP plant operating under CCS technology would release almost zero emissions of CO_2. However, a comprehensive cost analysis should be performed to check plant's economic feasibility. A simplified cost analysis is presented in the next section.

5. PRELIMINARY FEASIBILITY ANALYSIS

Brazil operates a large scale state-of-the-art thermoelectric power plant called 'UTE-LORM' comprised of 24 Wärtsilä 20V34SG gas generator sets with a total combined output of 204 MW [15].

Assuming an oxygen plant – coupled to that power plant (204 MW) – with a typical production cost of US$ 0.045/kg for high purity oxygen (>95%) obtained through cryogenic distillation process [13], the study points towards a payback time between 6 and 17 years depending on the OFC operating modes presented in table 4. Cost analysis refer to an oxy-fuel technology implementation on a CHP plant on a 24/7 basis.

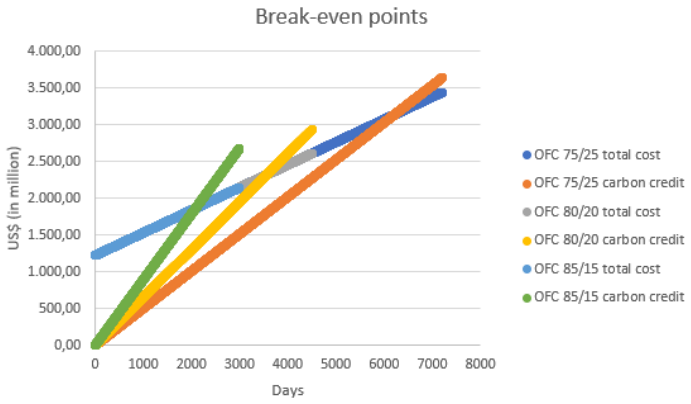

Fig. 2 – Break-even points for different OFC modes for a 204 MW power plant.

This figure was based on a carbon credit of US$ 36/stored CO_2 ton. The authors are elaborating a more detailed feasibility model that will be published in the near future.

6. CONCLUSIONS

A model was developed to estimate relevant gas engine performance parameters under oxy-fuel burning technology for carbon capture and storage of CHP plants.

Numerical predictions showed that oxy-fuel combustion of RDF pyrolysis gas in gas engines did not penalize system thermal efficiency. The exhaust gas temperature and heat content are suitable for combined heat and power plants under zero emissions operation.

A more detailed model for cost analysis should be included in the model for feasibility analysis under the carbon credit approach.

7. REFERENCE

7.1 References

[1] Boloy R, Silveira J, Tuna C, Coronado C, Antunes J. Ecological impacts from syngas burning in internal combustion engine: Technical and Economic aspects. Renewable and Sustainable Energy Reviews. 2011, Vol 15, pp. 5194-5201. DOI: 10.1016/j.rser.2011.04.009

[2] Van Blarigan A, Kozarac D, Seiser R, Cattolica R, Chen J-Y, Dibble R. Experimentaal Study of Methane Fuel Oxycombustion in a Spark Ignited Engine. Journal of Energy Resources Technology. 2013; 136:012203. https://doi.org/10.1115/1.4024974

[3] Serrano J, Arnau F, García-Cuevas L, Farias V. Oxy-fuel combustion feasibility of compression ignition engines using oxygen separation membranes for enabling carbon dioxide capture.

[4] E. Commission, 2030 climate and energy framework in European Union. Accessed on April 2th 2022. URL: https://ec.europa.eu/clima/policies/strategies/2030_en

[5] Xiang Li, Zhijun P, Ajmal T, Aitouche A, Mobasheri R, Pei Y, Gao Bo, Wellers M. A feasibility study of implementation of oxy-fuel combustion on a practical diesel engine at the economical oxygen-fuel ratios by computer simulation. Advances in Mechanical Engineering 2020, Vol 12(12) 1-13. DOI: 10.1177/1687814020980182.

[6] Wärtsilä. Combustion Engine vs Gas Turbine: Fuel Flexibility. Accessed April 12th, 2022. https://www.wartsila.com/energy/learn-more/technical-comparisons/combustion-engine-vs-gas-turbine-fuel-flexibility

[7] Boehman A, Le Corre O. Combustion of Syngas in Internal Combustion Engines. 180:6, 1193-1206, DOI: 10.1080/00102200801963417

[8] Copa J, Tuna C, Silveira J, Boloy R, Brito P, Silva V, Cardoso J, Eusébio D. Techno-Economic Assessment of the Use of Syngas Generated from Biomass to Feed an Internal Combustion Engine. Energies 2020, 13, 3097. DOI: 10.3390/en13123097

[9] Zhihua Wang. Zhihua Wang, 1.23 Energy and Air Pollution, Editor(s): Ibrahim Dincer, Comprehensive Energy Systems, Elsevier, 2018, Pages 909-949, ISBN 9780128149256, https://doi.org/10.1016/B978-0-12-809597-3.00127-9.

[10] Rayca P, Poskart A, Chrubasik M, Sajdak M, Zajemska M, Skibinski A, Korombel A. Technological and economic aspect of Refused Derived Fuel pyrolysis. Renewable Energy, Volume 161, 2020, Pages 482-494, ISSN 0960-1481, https://doi.org/10.1016/j.renene.2020.07.104.

[11] Martin J, Motores de Combustão Interna, Université Catholique de Louvain. UCL. TERM, 2008.

[12] EES,2022. Engineering Equation Solver, F-Chart Software, accessed April 8th, 2022. http://www.fchart.com/ees/

[13] Adhikari B, Orme C, Klaehn J, Stewart F. Technoeconomic analysis of oxygen-nitrogen separation for oxygen enrichment using membranes. Separation and Purification Technology 2021. Volume 268, ISSN 1383-5866, https://doi.org/10.1016/j.seppur.2021.118703.

[14] Caterpillar G3520E. Gas Engine Technical Data. Fuel Flexibility. Accessed April 25th 2022. https://emc.cat.com/pubdirect.ashx?media_string_id=GAS-DM8924-02-GS-EPG-M-13100177.pdf

[15] Wärtsilä. Gas and multi-fuel power plants. Accessed May 20th, 2022 https://cdn.wartsila.com/docs/default-source/power-plants-documents/downloads/brochures/gas-and-multi-fuel-power-plants-2017.pdf

Gmail **Andrew Cardoso <andrewccardoso@gmail.com>**

ICAE2022: Recommendation to the special issue of ICAE2022

14th International Conference on Applied Energy (ICAE2022) 13 de setembro de 2022 17:30
<noreply@xcdsystem.com>
Responder a: icae2022@applied-energy.org
Para: andrewccardoso@gmail.com

Dear Andrew Cardoso,

Based on the evaluations of the session chairs and the scientific committee of ICAE2022, we are pleased to inform you that your paper:

528: Gas engine Oxy Fuel Combustion for Combined Heat and Power Applications

presented at the 14th International Conference on Applied Energy, (ICAE2022), Aug 8-11, 2022 has been selected for the further consideration in Applied Energy and Advances in Applied Energy.

The submission will be open from Nov 1, 2022 and the DEADLINE for the submission to the Special Issue is May 31, 2023. You are free to choose the target journal, but we may transfer your paper depending on, for example, the scope and other plans. Please pay attention to the DEADLINE and carefully check the following issues when preparing your manuscript:

(1) Prepare the full paper following the Guide for Authors (APEN: https://www.elsevier.com/journals/applied-energy/0306-2619/guide-for-authors; ADAPEN: https://www.elsevier.com/journals/advances-in-applied-energy/2666-7924/guide-for-authors). The template of ICAE2022 shall NOT be used anymore.

(2) Carefully address originality and the relevance to applied energy issues. You are suggested to read previous published papers in Applied Energy and Advances in Applied Energy to understand the readership and scope of the journals. A proof reading by a native English speaker is suggested.

(3) Please clearly indicate your paper ID in the cover letter and mention that this paper is recommended to the SI:ICAE2022. Your submission will be returned to you if this is NOT added.

(4) A footnote should be added in the manuscript, indicating "The short version of the paper was presented at ICAE2022, Bochum, Germany, Aug 8-11, 2022. This paper is a substantial extension of the short version of the conference paper."

(5) To avoid the potential conflict in indexing system, a modified title and significant extension (**adding at least 50%**) of the text and content shall be conducted based on the conference paper.

(6) The final decision of the acceptance/rejection of the manuscript will be decided by Applied Energy and Advances in Applied Energy after review organized by the Journal.

(7) Please choose VSI:ICAE2022 when you submit your paper at https://www.editorialmanager.com/APEN/default.aspx and https://www.editorialmanager.com/adapen/default1.aspx

If you have any question, please contact us at icae2022@applied-energy.org.

Sincerely,

Prof J. Yan and Prof R. Span

Conference Chair of ICAE2022